Donor-Acceptor Binary Adducts of Tetrathiafulvalene Donors with Cyclic Trimetallic Monovalent Coinage Metal Acceptors

Mukunda M. Ghimire, [†, £] *Oumarou C. Simon,* [§, †] *Lauren M. Harris,* [†] *Annette Appiah,* [£] *Ryan M. Mitch,* [£] *Vladimir N. Nesterov,* [†] *Alceo Macchioni,* [‡] *Cristiano Zuccaccia,* [‡] *Hassan Rabaâ,* [‖] *Rossana Galassi,* [*, §], *and Mohammad A. Omary** [*, †, #]

[†]Department of Chemistry, University of North Texas, Denton, TX 76203, USA.

[£] Lebanon Valley College, Annville, PA-17003, USA.

[§]School of Science and Technology, Chemistry Division, University of Camerino, Via Sant'Agostino, 1, Camerino, I- 62032, Italy.

[‡]Department of Chemistry, Biology and Biotechnology, University of Perugia, Via Elce di Sotto 8, Perugia, I-06123, Italy.

[‖]Department of Chemistry, ESCTM, Ibn Tofail University, P.O. Box 133, Kenitra, 14000, Morocco.

[#] Department of Chemistry, Yarmouk University, Irbid 21163, Jordan

ABSTRACT

The reactions between the π-acidic cyclic trimetallic coinage metal(I) complexes {[Cu(μ-3,5-$(CF_3)_2$pz)]$_3$, {[Ag(μ-3,5-$(CF_3)_2$pz)]$_3$, and {[Au(μ-3,5-$(CF_3)_2$pz)]$_3$ with TTF, DBTTF and BEDT-TTF give rise to a series of coinage metal(I)-based new binary donor-acceptor adducts {[Cu(μ-3,5-$(CF_3)_2$pz)]$_3$DBTTF} = **1**, {[Ag(μ-3,5-$(CF_3)_2$pz)]$_3$DBTTF} = **2**, {[Au(μ-3,5-$(CF_3)_2$pz)]$_3$DBTTF} **= 3**, {[Cu(μ-3,5-$(CF_3)_2$pz)]$_3$TTF} = **4**, {[Ag(μ-3,5-$(CF_3)_2$pz)]$_3$TTF} = **5**, {[Au(μ-3,5-$(CF_3)_2$pz)]$_3$TTF} = **6**, {[Cu(μ-3,5-$(CF_3)_2$pz)]$_3$BEDT-TTF}= **7**, {[Ag(μ-3,5-$(CF_3)_2$pz)]$_3$BEDT-TTF} = **8**, and {[Au(μ-3,5-$(CF_3)_2$pz)]$_3$BEDT-TTF} = **9**, (where pz = pyrazolate, TTF = tetrathiafulvalene , DBTTF = dibenzotetrathiafulvalene , and BEDT-TTF = bis(ethylenedithio)tetrathiafulvalene). This series of binary donor-acceptor adducts have been found to exhibit remarkable supramolecular structures in both the solid state and solution, whereby they exhibit supramolecular stacked chains and oligomers, respectively. The supramolecular solid and solution binary donor-acceptor adducts also exhibit superior shelf stability under ambient laboratory storage conditions. Structural and other electronic properties of solid and solutions of these adducts have been characterized by single crystal X-ray diffraction structural analysis. ^{1}H and ^{19}F NMR, UV-Vis-NIR spectroscopy, FTIR, and computational investigations. The combined results of XRD structural data analysis spectroscopic measurements and theoretical studies suggest the sustenance of the donor-acceptor stacked structure and electronic communication in both the solid state and solution. These properties are discussed in terms of potential applications for this new class of supramolecular binary donor-acceptor adducts in molecular electronic devices, including solar cells, magnetic switching devices, and field effect transistors.

INTRODUCTION

Recently, much attention has been given to molecule-based devices, predominantly photovoltaics solar cells, molecular-magnets, conductors, and superconductors.[1-8] The potential these devices to bring about technical revolution in key industrial areas such as environment and energy, medical care, electronics, and transportation has been suggested.[2-8] Several classes of charge transfer complexes have been designed and synthesized toward this purpose whereby binary donor-acceptor supramolecular structures exhibit π- π and *d*-π interactions.[2-4] These organic-inorganic binary donor-acceptor adducts can offer several advantages over their purely organic-counterpart. The enhancement of intermolecular interactions by quadrupolar electrostatic interactions in these supramolecular structures can increase dimensionality and suppress metal-insulator transitions.[1-6] Such electrostatic interactions can also lead to the formation of unique molecular networks that afford special functions such as inclusion properties, which could lead to "clean energy" applications upon designated host-guest interactions.[7] Similarly, strong intermolecular charge transfer interactions are expected for supramolecular structures toward crystal engineering, en route to achieving desirable donor-acceptor morphologies that exhibit a particular function intuitively.[2-7]

One particularly intriguing result in this area has been demonstrated by Tanaka *et al.* by preparing a superconducting molecular "synthetic metallic crystal" salt based on $[Ni(dmit)_2]^{2-}$, where dmit = 2-thioxo-1,3-dithiole-4,5-dithiolate, which can form a charge transfer complex with either an open- or closed-shell organic cation.[8] Several other recent reports have initiated renewed interest in charge transfer complexes by highlighting a variety of properties arising at the interface between the donor and acceptor molecules that were not

offered by either of the parent molecules. For example, Dunbar, Omary and co-workers reported supramolecular stacks of neutral (diimine)(dithiolato)platimum(II) ambipolar complexes with nitrile- or nitrofluorenone-based acceptors that exhibit favorable properties for solar cell applications with strong absorptions across a wide spectral range, some of which have been validated for photocurrent generation.[9] In separate spectroscopic and electronic structure studies by the same groups, [Pt(tbtrpy)X]Y complexes -- where X = Cl, NCS, OH, or various arylthiolates and $Y^- = Cl^-$, BF_4^-, or $TCNQ^-$ = 7,7,8,8-tetracyanoquinodimethane radical anion -- demonstrated that varying the anionic ligand X and/or counterion Y^- can be fine- or coarse-tuned to attain red-shifts in various charge transfer absorption bands to the visible and near-infrared regions.[10] Other notable examples include a novel study of intermolecular interactions in the molecular ferromagnetic $NH_4Ni(mnt)_2.H_2O$ (mnt = maleonitrile) complex, as reported by Coomber et al.[11] Other relevant studies by Balch et al. and by some of us have suggested the ability of cyclic trimetallic Au(I) complexes to function as electron donors.[12a-c] Several supramolecular binary adducts of these electron-rich gold(I) complexes were isolated with well-known neutral organic electron acceptors or π-acids such as polynitro-9-fluorenones[12a] or neutral TCNQ and C_6F_6 molecules,[12b] an organometallic perfluorinated π-acid,[12c] or heavy metal cations.[12d] Moreover, Alvarez et al. have outlined a significant aspect of the solid-state interactions in similar hybrid organic-inorganic materials, in terms of the overlap of the diffuse π-orbitals on the sulfur atoms with the metal d-orbitals.[13]

In their limiting cases, donor/acceptor stacks can be either segregated or integrated in charge-transfer materials with distinct properties -- as conductors or magnets for segregated or integrated stacks, respectively, that are most commonly studied for such stacks of metal-free organic molecules typified by tetrathiafulvalene donors and nitrile acceptors.[1-8] However, the involvement of d orbitals in metal-containing donor-acceptor stacks may impart either or both

properties without correlation to the stacking type, as well as sensitize other properties such as photo- or electro-luminescence, sensors, and photovoltaic solar cells.[9-14]

Chart 1. Acceptors (left) A1 = [Cu(μ 3,5-$(CF_3)_2$pz)]$_3$; A2 = [Ag(μ 3,5-$(CF_3)_2$pz)]$_3$; and A3 = [Au(μ 3,5-$(CF_3)_2$pz)]$_3$ and donors (right) D1 = tetrathiafulvalene (TTF); D2 = dibenzotetrathiafulvalene (DBTTF); and D3 = bis(ethylenedithio)tetrathiafulvalene (BEDT-TTF).

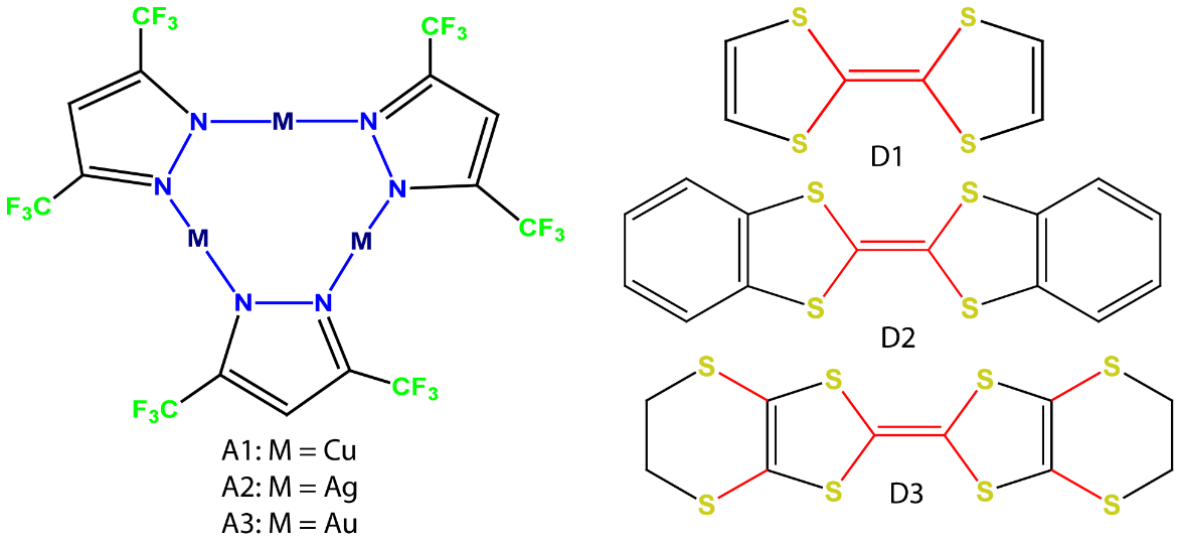

In this project, we have successfully co-assembled π-acidic cyclic trimetallic coinage metal(I) acceptor complexes (Chart 1, left) A1 = [Cu(μ 3,5-$(CF_3)_2$pz)]$_3$; A2 = [Ag(μ 3,5-$(CF_3)_2$pz)]$_3$; and A3 = [Au(μ 3,5-$(CF_3)_2$pz)]$_3$ with organic donor molecules (Chart 1, right)- D1 = tetrathiafulvalene (TTF); D2 = dibenzotetrathiafulvalene (DBTTF); and D3 = bis(ethylenedithio)tetrathiafulvalene (BEDT-TTF) to yield nine new types of molecular and supramolecular binary donor-acceptor adducts; {[Cu(μ-3,5-$(CF_3)_2$pz)]$_3$DBTTF} = **1**, {[Ag(μ-3,5-$(CF_3)_2$pz)]$_3$DBTTF} = **2**, {[Au(μ-3,5-$(CF_3)_2$pz)]$_3$DBTTF} = **3**, {[Cu(μ-3,5-$(CF_3)_2$pz)]$_3$TTF} = **4**, {[Ag(μ-3,5-$(CF_3)_2$pz)]$_3$TTF} = **5**, {[Au(μ-3,5-$(CF_3)_2$pz)]$_3$TTF} = **6**, {[Cu(μ-3,5-$(CF_3)_2$pz)]$_3$BEDT-TTF}= **7**, {[Ag(μ-3,5-$(CF_3)_2$pz)]$_3$BEDT-TTF} = **8**, and

{[Au(μ-3,5-$(CF_3)_2$pz)]$_3$BEDT-TTF} = **9** with interesting opto-electronic properties. This paper reports comprehensive experimental and theoretical studies of these charge transfer binary donor-acceptor adducts whereby we describe their syntheses, solid-state structural characterization, spectroscopic studies, and computational analysis of their electronic structure. Apart from their relevance as conducting and magnetic materials, some of these complexes are also interesting from the perspective of their electronic absorption, as demonstrated by this work for their potential use in molecular devices as conductors.

EXPERIMENTAL METHODS

Materials and methods. All the air-sensitive synthetic steps were performed under inert atmosphere using Standard Schlenk technique. Solvents used were dried and degassed prior to use. Deuterated solvents were purchased from Sigma–Aldrich and Cortecnet and used as received. 3, 5-bis(trifluoromethyl)pyrazole, TTF, DBTTF, and BEDT-TTF were purchased from vendors and used without any further purification. {[Cu(μ-3,5-$(CF_3)_2$pz)]$_3$, {[Ag(μ-3,5-$(CF_3)_2$pz)]$_3$, and {[Au(μ-3,5-$(CF_3)_2$pz)]$_3$ was synthetized as described in the previously reported literatures.[15-18]

Physical Measurements. Nuclear magnetic resonance (NMR) spectra were recorded on a Varian-NMR spectrometer operating at 500 MHz or on a Bruker Avance III HD instrument equipped with a smart probe operating at 400 MHz. All measurements were performed at 298 K unless otherwise stated. Chemical shifts are reported relative to external Me_4Si using the residual proton resonance of the deuterated solvent as internal reference. The multiplicity of signals is described using the following abbreviations: br = broad, d = doublet, dd = double doublet, t = triplet, m = multiplet, s = singlet. 1D ^{1}H, ^{19}F HOESY NMR measurements were

carried out in cyclohexane-d_{12} at 333 K using a relaxation delay of 2s and a mixing time of 800 ms.

The Mid- infrared (IR) spectra were collected on a Thermo-Scientific Nicolet-6700 Fourier Transform-Infrared (FTIR) spectroscopy with a smart orbit diamond attenuated total reflectance (ATR) accessory by firmly pressing the neat sample onto the diamond plate of the ATR accessory to record spectra from 4000 to 600 cm^{-1}. A Perkin-Elmer SPECTRUM ONE System FT-IR instrument was also used to collect the spectra. UV-Vis-NIR absorption measurements of dichloromethane solution of adducts **1-9** were carried out using a PerkinElmer Lambda 900 spectrophotometer using suprasil quartz cuvettes with 10 mm path lengths. The solid reflectance data was collected using the LabSphere integrating sphere accessory to the Lambda 900 spectrophotometer which is connected to Peltier system for temperature dependent experiments. Electrospray ionization mass spectrometry (ESI-MS) spectra were obtained in positive- or negative-ion mode on the 1100 series MSD detector HP spectrometer, using an acetonitrile mobile phase. The compounds were added to reagent-grade acetonitrile to give solutions with approximate concentrations of 0.1 mM. These solutions were injected (1 μL) into the spectrometer via a HP 1090 series II high performance liquid chromatography (HPLC) instrument, fitted with an auto-sampler. The pump delivered the solutions to the mass spectrometer source at a flow rate of 300 μL min^{-1}, and nitrogen was employed as both a drying and nebulizing gas. Capillary voltages were typically 4000 and 3500 V for the positive- and negative-ion modes, respectively. Confirmation of all major species in this ESI-MS study was aided by a comparison of the observed and predicted isotope distribution patterns, with the latter calculation using the IsoPro 3.0 program. Elemental analyses (C, H, N, and S) were performed in-house with a Fisons Instrument 1108 CHNS-O

elemental analyzer. An SMP3 Stuart Scientific Instrument, and an Electrothermal Mel-Temp melting point device were used to determine the melting point.

X-ray Crystallographic Determination. Crystal structure determination for all complexes were carried out using a Bruker SMATR APEX2 CCD-based X-ray diffractometer equipped with a low temperature device and Mo-target X-ray tube (wavelength = 0.71073 Å). Measurements were taken at 296(2) K and 220(2) K. Data collection, indexing, and initial cell refinements were carried out using APEX2,[19] frame integration and final cell refinements were done using SAINT.[20]An absorption correction was applied using the program SADABS.[21]All non-hydrogen atoms were refined anisotropically. The hydrogen atoms in the complexes were placed in idealized positions and were refined as riding atoms. Structure solution, refinement, graphic and generation of publication materials were performed by using SHELXTL software.[22]

Solid-State and Molecular Simulations. The solid-state electronic structure calculations are performed within the framework of the extended Hückel tight binding (EHTB) method, [23] for which standard parameters are used within the YAeHMOP[24] software package. The off-diagonal elements of the Hamiltonian are evaluated with the Wolfsberg-Helmholtz formula.[25] Numerical integrations over the symmetry unique section of the Brillouin zone of the three-dimensional structures of the donor-acceptor complexes were performed using a set of 56 k-points. The Gaussian 09 program[26] was used for the preliminary density functional calculations that utilized the LANL2DZ valence basis sets and compact effective potentials[27] in conjunction with the B3LYP hybrid functional,[28] whereas higher-accuracy calculations utilized the Turbomole package for geometry optimization using the TPSS/Def2 functional/basis set combination with the Grimme dispersion applied.[29]

Syntheses. Crystalline charge-transfer binary donor-acceptor adducts **1-9** were obtained by mixing the components as dichloromethane solutions, followed by the purification that are described in detail below**:**.

*Synthesis of {[Cu(μ-3,5-(CF$_3$)$_2$pz)]$_3$DBTTF}, **1***

To a stirring 10 mL CH_2Cl_2 solution containing 30 mg (0.037 mmol) of [Cu-(μ-3, 5-CF_3)$_2$pz]$_3$ in a Schlenck flask11.45 mg (0.037 mmol) of solid DBTTF was added under inert N_2 environment. The colorless solution turned yellow. Resulted yellow-colored solution was stirred overnight at room temperature. Afterward, the reaction mixture was filtered, and the solvent was removed under reduced pressure to give a bright yellow solid. The solid was washed with hexane (3 × 5 mL), dried and recrystallized in a mixture of dichloromethane and hexane to give yellow needles as single crystals of suitable quality for X-ray solid state single crystal structural determination. {[Cu(μ-3,5-(CF$_3$)$_2$pz)]$_3$DBTTF}: Yield: 85 %; M. p. > 250; ^{1}H-NMR (CD_2Cl_2, 298K) δ: 7.25 (br) 7.05 (s); ^{19}F-NMR (CD_2Cl_2, 298K) δ: -61.02 (s); ^{1}H-NMR (CD_2Cl_2, 298K, saturated solution) δ: 7.16 (br), 6.99 (s); ^{19}F-NMR (CD_2Cl_2, 298K, saturated solution) δ: -60.96 (s); ESI(+) (CH_3OH): m/z: 102.2 (50), 274.4 (100), 304.0 (40) $[DBTTF+H]^+$, 722.7 (15), 764.7 (10); ESI(-): 203.0 (45) $[3,5\text{-}(CF_3)_2\text{-}pz]^-$, 469.0 (20), 834.7 (100), 1002.8(40); IR (cm^{-1}): 3150.7(w), 3055.4(w), 2964.4(w), 1643.1(w), 1540.7(s), 1506.6(s), 1450.1(vs), 1362.2(s), 1226.4(s), 1256.1(vs), 1121.7(br), 1099(w), 1031.9(vs), 991.4(s), 933.0(m), 816.2(vs), 776.3, 759.0(w), 735.7(w), 744.9(vs), 674.6(s); Elemental analysis for $C_{29}H_{11}Cu_3F_{18}N_6S_4$ (%), calc.: C, 31.54; H, 1.00, N, 7.61; S, 11.61; found: C, 31.5819; H, 1.1101; N, 6.3809; S, 11.6534.

*Synthesis of {[Ag(μ-3,5-(CF$_3$)$_2$pz)]$_3$DBTTF}, **2***

To a stirring 10 mL CH_2Cl_2 solution containing 30 mg (0.032 mmol) of [Ag(μ -3,5-$(CF_3)_2$pz]$_3$ in a Schlenck flask, 9.7 mg (0.032 mmol) of DBTTF was added under inert N_2 environment. After few minutes, a pale-yellow suspension was formed, and the reaction mixture was stirred overnight at room temperature. The suspension was then centrifuged to separate the solid from the solution. The crude yellow solid was dried under vacuum, dissolved in acetone and by slow evaporation yellow needles crystals of single crystal X-ray quality were obtained after couple of days. {[Ag(μ-3,5-$(CF_3)_2$pz)]$_3$DBTTF}: Yield: 80.58%. M. p. > 250; ^{1}H-NMR (CD_2Cl_2, 298K, saturated solution) δ: 7.22 (br), 7.03 (br); ^{19}F-NMR (CD_2Cl_2, 298K, saturated solution) δ: -61.26 (s) ESI (+) (CH_3OH), m/z: 102.2 (50), 274.4 (100), 304.0 (40) $[DBTTF+H]^+$, 722.7 (20); ESI(-), 203.0 (100) [3,5-$(CF_3)_2$-pz]$^-$, 325.1 (20). IR (cm^{-1}): 3146.8, 3075.6, 1951.5, 1901.3, 1855.3, 1629.6, 1569.0, 1547.7, 1530.1, 1449.7, 1354.3, 1235.0, 1180.0, 1153.0, 1117.8, 1088.1, 1020.7, 987.8, 976.5, 935.0, 813.2, 775.7, 745.8, 734.7, 712.8, 673.9; Elemental analysis for $C_{29}H_{11}Ag_3F_{18}N_6S_4$ (%), calc.: C, 28.15; H, 0.90; N, 6.79; S, 10.37; found: C, 28.31; H, 0.89; N, 6.16; S, 10.09.

Synthesis of {[Au(μ-3,5-$(CF_3)_2$pz)]$_3$DBTTF}, ***3***

To a stirring 10 mL CH_2Cl_2 solution containing 30 mg (0.025 mmol) of [Au(μ-3,5-$(CF_3)_2$pz]$_3$ in a Schlenck flask, 7.6 mg (0.025 mmol) of solid DBTTF was added under inert N_2 environment. The reaction mixture was stirred overnight at room temperature. Afterward, the reaction mixture was filtered, and the solvent was removed under reduced pressure to give a bright yellow solid. The solid was washed with hexane (3 × 5mL), dried and recrystallized in a mixture of dichloromethane and hexane to give yellow needles as crystals suitable for X-ray single crystal structural analysis. {[Au(μ-3,5-$(CF_3)_2$pz)]$_3$DBTTF}: Yield: 45.58%; M. p. > 250; ^{1}H-NMR (CD_2Cl_2, 298K): δ 7.18 (very br); ESI(+) (CH_3OH), m/z: 303.9 (100)

[DBTTF+H]$^{+}$, 337.0 (10); ESI(-), 434.9 (40), 516.9 (10); 602.9 (100); IR (cm^{-1}): 3145.8, 3081.8, 3056.2, 1943.0, 1900.5, 1860.4.3, 1645.8, 1553.5, 1539.7, 1499.8, 1450.6, 1441.3, 1392.1, 1377.1, 1256.2, 1135.5, 1119.8, 1040.4, 991.6, 929.6, 819.0, 776.1, 765.2, 711.6, 675.1; Elemental analysis for $C_{29}H_{11}Au_3F_{18}N_6S_4$ (%), calc.: C, 23.15; H, 0.74; N, 5.59; S, 8.52; found: C, 23.91; H, 0.79; N, 5.16; S, 8.09.

Synthesis of {[Cu(μ-3,5-(CF$_3$)$_2$pz)]$_3$TTF}, ***4***

To a stirring 10 mL CH_2Cl_2 solution containing 30 mg (0.037mmol) of [Cu(μ-3,5-CF_3)$_2$pz]$_3$ in a Schlenck flask, 8 mg (0.037 mmol) of solid TTF was added under inert N_2 environment. The yellow solution was then, stirred overnight at room temperature. Afterward, the reaction mixture was filtered, and the solvent was removed under reduced pressure to give a bright yellow solid. The solid was washed with hexane (3 × 5 mL), dried and recrystallized in a mixture of dichloromethane and hexane to give yellow needles as crystals. {[Cu(μ-3,5-(CF$_3$)$_2$pz)]$_3$TTF}:Yield: 75 %; M. p. > 250; ^{1}H-NMR (CD_2Cl_2, 298K) δ; 7.07 (very br); ^{19}F-NMR (CD_2Cl_2, 298K) δ: -60.95 (s); IR (cm^{-1}): 3156.6(w), 3092.7(w), 1643.1(w), 1542.7(w), 1554.7(w), 1539.8(wbr), 1506.9(s), 1455.8(vs), 1363.8(s), 1226.4(s), 1255.5(vs), 1116.3(br), 1099(w), 1031.5(vs), 991.6(s), 820.2(vs), 793.3(m), 779.5(w), 758.8(s), 735.0(s), 714.1(s); Elemental analysis for ($C_{19}H_9Cu_3F_{12}N_6S_4$) (%), calc.: C, 26.28; H, 1.04; N, 9.68; S, 14.77; found: C, 25.9856; H, 1.1234; N, 9.7654; S, 14.8765.

Synthesis of {[Ag(μ-3,5-(CF$_3$)$_2$pz)]$_3$TTF}, ***5***

To a stirring 10 mL CH_2Cl_2 solution containing 30 mg (0.037mmol) of [Ag-(μ-3,5-CF_3)$_2$pz]$_3$ in a Schlenck flask, 8 mg (0.037 mmol) of TTF was added under inert N_2 environment. The yellow solution was stirred overnight at room temperature. The resulted

reaction mixture was then filtered, and the solvent was removed under reduced pressure to give a bright yellow solid. The solid was washed with hexane (3 × 5 mL), dried and recrystallized in a mixture of dichloromethane and hexane to give yellow needles as crystals. {[Ag(μ-3,5-$(CF_3)_2$pz)]$_3$TTF}:Yield: 75 %; M. p. > 250; ^{1}H-NMR (CD_2Cl_2, 298K) δ: 6.99 (very br); ^{19}F-NMR (CD_2Cl_2, 298K) δ: -61.32 (s); IR (cm^{-1}): 3152.4(w), 3098.4(w), 1634.6(w), 1549.6(w), 1531.5(w), 1505.3(s), 1453.8(w), 1354.1(s), 1251.5(vs), 1233.8(w), 1116.0(br), 1088.4(w), 1019.5(vs), 987.4(s), 861.9(w), 815.8(vs), 793.1(s), 778.8(w), 755.9(s), 733.9(s), 713.2(s); Elemental analysis for ($C_{19}H_9Ag_3F_{12}N_6S_4$) (%), calc.: C, 26.79; H, 0.91; N, 8.39; S, 12.81; found: C, 26.6543; H, 0.9234; N, 8.4232; S, 12.7634.

Synthesis of {[Au(μ-3,5-$(CF_3)_2$pz)]$_3$TTF}, ***6***

To a stirring 10 mL CH_2Cl_2 solution containing 30 mg (0.025 mmol) of [Au-(μ -3,5-$(CF_3)_2$pz]$_3$ in a Schlenck flask, 5.1 mg (0.025 mmol) of solid DBTTF was added under inert N_2 environment. The reaction mixture was stirred overnight at room temperature. The resulted reaction mixture was then filtered, and the solvent was removed under reduced pressure to give yellow solid. The crude product was recrystallized in a mixture of dichloromethane and hexane to give yellow needles as crystals. {[Au(μ-3,5-$(CF_3)_2$pz)]$_3$TTF}: Yield: 45.58%; M. p. > 250; ^{1}H-NMR (CD_2Cl_2, 298K) δ: 6.89 (very br); IR (cm^{-1}): 3145.8, 3081.8, 3056.2, 1943.0, 1900.5, 1860.4.3, 1645.8, 1553.5, 1539.7, 1499.8, 1450.6, 1441.3, 1392.1, 1377.1, 1256.2, 1135.5, 1119.8, 1040.4, 991.6, 929.6, 819.0, 776.1, 765.2, 711.6, 675.1; Elemental analysis for $C_{21}H_7Au_3F_{18}N_6S_4$ (%), calc.: C, 17.96; H, 0.50; N, 5.98; S, 9.13; found: C, 18.0652; H, 0.5321; N, 5.8762; S, 9.0123.

Synthesis of {[Cu(μ-3,5-$(CF_3)_2$pz)]$_3$BEDT-TTF}, ***7***

To a stirring 10 mL CH_2Cl_2 solution containing 30 mg (0.037mmol) of [Cu-(μ-3,5-CF_3)$_2$pz]$_3$ in a Schlenck flask, 14 mg (0.037 mmol) of solid BEDT-TTF was added under inert N_2 environment. The orange solution was stirred for 2 days at room temperature. Afterward, the reaction mixture was filtered, and the solvent was removed under reduced pressure to give a bright orange solid. The solid was washed with hexane (3 × 5 mL), dried and recrystallized in a mixture of dichloromethane and hexane to give orange needles as crystals. {[Cu(μ-3,5-(CF_3)$_2$pz)]$_3$BEDT-TTF}: Yield: 65 %; M. p. > 250; ^{1}H-NMR (CD_2Cl_2, 298K) δ 7.02 (s), 3.97(m); IR (cm^{-1}): 3162(w), 2964(w), 2919(w) 1666(w), 1543(s), 1507(s), 1456(m), 1362(s), 1255(vs), 1232(m), 1116(br), 1026(vs), 823(vs), 759(vs), 735(m), 715(s); Elemental analysis for ($C_{25}H_{11}Cu_3F_{18}N_6S_8$) (%), calc.: C, 25.35; H, 0.94; N, 7.09; S, 21.66; found: C, 25.4543; H, 0.9234; N, 6.9985; S, 21.5678.

Synthesis of {[Ag(μ-3,5-(CF_3)$_2$pz)]$_3$BEDT-TTF}, ***8***

To a stirring 10 mL CH_2Cl_2 solution containing 30 mg (0.032mmol) of [Ag-(μ-3,5-CF_3)$_2$pz]$_3$ in a Schlenck flask, 12 mg (0.032 mmol) of solid BEDT-TTF was added under inert N_2 environment. The orange solution was then stirred for 2 days at room temperature. The resulted reaction mixture was filtered, and the solvent was removed under reduced pressure to give a bright orange solid. The solid was washed with hexane (3 × 5mL), dried and recrystallized in a mixture of dichloromethane and hexane to give orange needles as crystals. {[Ag(μ-3,5-(CF_3)$_2$pz)]$_3$BEDT-TTF}: Yield:70%; M.p> 250; IR (cm^{-1}): ^{1}H-NMR (CD_2Cl_2, 298K) δ: 6.97 (s), 3.54 (m); IR (cm^{-1}): 3141.4(w), 2962.4(wbr) 2926.0(wbr), 2852.3(wbr), 1625.0(w), 1547.3(m), 1530.8(m), 1502.7(s), 1353.3(s), 1250.8(s), 1229.1(w), 1116.0(s), 1017.0(vs), 917.0, 882.0, 812.0(vs), 755.9; Elemental analysis for ($C_{25}H_{11}Ag_3F_{18}N_6S_8$) (%), calc.: C, 22.79; H, 0.84; N, 6.38; S, 19.47; found: C, 23.6037; H, 0.8037; N, 6.035; S, 19.2320.

*Synthesis of {[Au(μ-3,5-$(CF_3)_2$pz)]$_3$BEDT-TTF}, **9***

To a stirring 10 mL CH_2Cl_2 solution containing 30 mg (0.025mmol) of [Au-(μ-3,5-$CF_3)_2$pz]$_3$ in a Schlenck flask, 9.6 mg (0.025 mmol) of BEDT-TTF was added under inert N_2 environment. The orange solution was stirred for 2 days at room temperature. Afterwards, the reaction mixture was filtered, and the solvent was removed under reduced pressure to give a bright orange solid. The solid was washed with hexane (3 × 5 mL), dried and recrystallized in a mixture of dichloromethane and hexane to give orange needles as crystals. {[Au(μ-3,5-$(CF_3)_2$pz)]$_3$BEDT-TTF}: Yield: 35 %; M.p. > 250; ^{1}HNMR (CD_2Cl_2, 298K) δ: 7.07 (s), 3.96(m); IR (cm^{-1}): 3147., 2962.4(wbr) 2926.0(wbr), 2852.3(, 1943.0, 1900.5, 1860.4.3, 1645.8, 1553.5, 1539.7, 1499.8, 1450.6, 1441.3, 1392.1, 1377.1, 1256.2, 1135.5, 1119.8, 1040.4, 991.6, 929.6, 819.0, 776.1, 765.2, 711.6, 675.1; Elemental analysis for $C_{25}H_{11}Au_3F_{18}N_6S_4$ (%), calc.: C, 22.79; H, 0.84; N, 6.38; S, 19.47; found: C, 22.45; H, 0.78; N, 6.47; S, 19.31.

RESULTS AND DISCUSSION

Synthetic Chemistry. The reaction of the π-acidic cyclic trimetallic complexes {[Cu(μ-3,5-$(CF_3)_2$pz)]$_3$, {[Ag(μ-3,5-$(CF_3)_2$pz)]$_3$, and {[Au(μ-3,5-$(CF_3)_2$pz)]$_3$ with TTF, DBTTF and BEDT-TTF resulted charge transfer binary donor-acceptor adducts **1-9**. These complexes are stable at room temperature and show their stabilities in air and light after days of exposure. Most of these complexes are soluble in dichloromethane, acetone, benzene, cyclohexane and chloroform. The synthetic procedure consists of the dissolution of the cyclic trimetallic coinage metal(I) complexes in CH_2Cl_2, followed by the addition of the organic donors. The resulted mixtures then stirred at room temperature under inert gas as described earlier, to give charge

transfer complexes in good percentage yield. These complexes are further characterized by crystallographic and spectroscopic studies, which will be discussed below.

Structural Characterization by X-ray Diffraction. Crystal data for charge transfer binary donor-acceptor adducts **1-5** and **8** are listed in **Table 1**. X-ray quality crystals were grown by slow evaporation of dichloromethane/hexane solutions for these binary donor-acceptor adducts. **Figures 1 – 6** shows the solid-state molecular structures of these complexes. The crystallographic data suggest that all of these complexes exhibit significant donor-acceptor or charge transfer interactions in the solid-state, as judged by the interplanar distances between the donor molecule and the acceptor molecules. Interplanar distances of 3.75 Å between the donor and acceptor molecules are close enough for the π-π, *d*-π and the electrostatic donor-acceptor interactions.[8-14]

Table 1. Crystallographic data and refinement parameters for charge-transfer complexes **1-5** and **8**.

Complexes	**1**	**2**	**3**
Formula	$C_{29}H_{11}Cu_3F_{18}N_6S_4$	$C_{29}H_{11}Ag_3F_{18}N_6S_4$	$C_{29}H_{11}Au_3F_{18}N_6S_4$
MW	1104.30	1237.29	1504.58
T (K)	296(2)	220(2)	220(2)
cryst syst	Monoclinic	Monoclinic	Monoclinic
space group	C 2/c	C 2/c	C 2/c
a (Å)	20.128(2)	20.4559(8)	20.6379(10)
b (Å)	13.9336(15)	13.8514(8)	13.7210(7)
c (Å)	14.3856(15)	14.2511(7)	14.6029(7)
α (deg)	90	90	90

β (deg)	113.355(2)	114.143(2)	116.851(1)
γ (deg)	90	90	90
V (Å^3)	3703.9(7)	3684.7(3)	3689.3(3)
Z	4	4	4
D_{calcd} (Mg m^{-3})	1.980	2.230	2.709
μ (mm^{-1})	2.058	1.932	12.253
reflns measured	24788	69266	46027
reflns unique [R_{int}]	4095 [0.0367]	4073 [0.0253]	4077 [0.0286]
R_1, wR_2 [$I > 2\sigma(I)$]	0.0391, 0.0998	0.0237, 0.0710	0.0152, 0.0452
R_1, wR_2 (all data)	0.0567, 0.1112	0.0255, 0.0742	0.0185, 0.0486
GOF on F^2	1.054	1.019	1.024
Complexes	**4**	**5**	**8**
Formula	$C_{21}H_7Cu_3F_{18}N_6S_4.H_2O$	$C_{21}H_7Ag_3F_{18}N_6S_4$	$C_{25}H_{11}Ag_3F_{18}N_6S_8$
MW	1022.20	1137.18	1317.49
T (K)	220(2)	220(2)	220(2)
cryst syst	Monoclinic	Triclinic	Monoclinic
space group	C 2/c	P -1	P 21/n
a (Å)	22.727(4)	12.223(1)	9.3315(7)
b (Å)	12.092(2)	12.817(2)	35.549(3)
c (Å)	24.783(4)	12.977(1)	12.1940(8)
α (deg)	90	96.133(3)	90
β (deg)	107.387(3)	116.919(2)	106.138(2)
γ (deg)	90	109.030(3)	90
V (Å^3)	6499.3(18)	1633.7(3)	3885.7(5)
Z	8	2	4

D_{calcd} (Mg m^{-3})	2.089	2.312	2.252
μ (mm^{-1})	2.338	2.167	2.046
reflns measured	41138	38793	80040
reflns unique [R_{int}]	9546 [0.0296]	7220 [0.0238]	8559 [0.0344]
R_1, wR_2 [$I > 2\sigma(I)$]	0.0914, 0.2662	0.0440, 0.1317	0.0499, 0.1481
R_1, wR_2 (all data)	0.1212, 0.3065	0.0501, 0.1387	0.0571, 0.1543
GOF on F^2	1.088	1.015	1.063

$$R_1 = \Sigma||F_o| - |F_c||/\Sigma|F_o| \text{ and } {}_wR_2 = \{\Sigma[w(F_o{}^2 - wF_c{}^2)^2/\Sigma[w(F_o{}^2)^2]\}^{1/2}$$

Structure of {[Cu(μ-3,5-$(CF_3)_2$pz)]$_3$DBTTF}, 1. The solid-state crystal structure of the charge transfer binary donor-acceptor adduct {[Cu(μ-3,5-$(CF_3)_2$pz)]$_3$DBTTF}, **1**, reveals that binary donor-acceptor adduct **1** crystalizes in the monoclinic space group C2/c and occupies a special position in the asymmetric unit (inversion center and two-fold axes, respectively). The solid-state crystal structure is depicted in **Figure 1 (a)** together with the atom numbering scheme. The DBTTF donor molecule and the cyclic trimetallic Cu(I) complex are stacked in an integrated pattern above and below each other, which allows for enhanced orbital overlap. The acceptor molecules are centered toward the sulfur atoms of the donor molecules resulting in a zig-zag extended packing motif. There are four Cu···S contacts above and below each donor molecule, interacting with acceptor molecule which are less than 4.0 Å as shown in **Figure 1** (**d**). The significant Cu···S interactions are 3.334(1) Å, 3.463(1) Å, 3.741(1) Å and 3.788(1) Å. The illustration of the calculated centroid···centroid interactions is given in **Figure 1** (**b**) and the infinite zig-zag chain of the donor-acceptor stack is shown in **Figure 1** (**c**). The orientation of the DBTTF molecules are in two different crystallographic spaces, where the next

neighboring DBTTF molecules in the stacks are always nearly perpendicular to one another throughout the extended structures as shown in **Figure 1** (**c**).

There is no any significant intermolecular metallophilic interaction between two adjacent cyclic trimetallic complexes. The extended supramolecular structures are mainly mediated by Cu···S interactions. The distances between the donor and acceptor molecules are well within the range of *d*-π interactions (3.750 Å). The organic donor DBTTF molecule adopts the similar packing arrangement herein, irrespective of the acceptor precursor, displays the favorable interactions between the cyclic trimetallic coinage metal(I) complexes as acceptor and DBTTF as organic donor molecules. Therefore, the stacking motif (D-A-D-A) of the donor-acceptor adduct {[Cu(μ-3,5-$(CF_3)_2$pz)]$_3$DBTTF}, **1**, signifies the energy stabilization that resulted from the interactions between the D-A molecules in this supramolecular stack of {[Cu(μ-3,5-$(CF_3)_2$pz)]$_3$DBTTF},**1**.

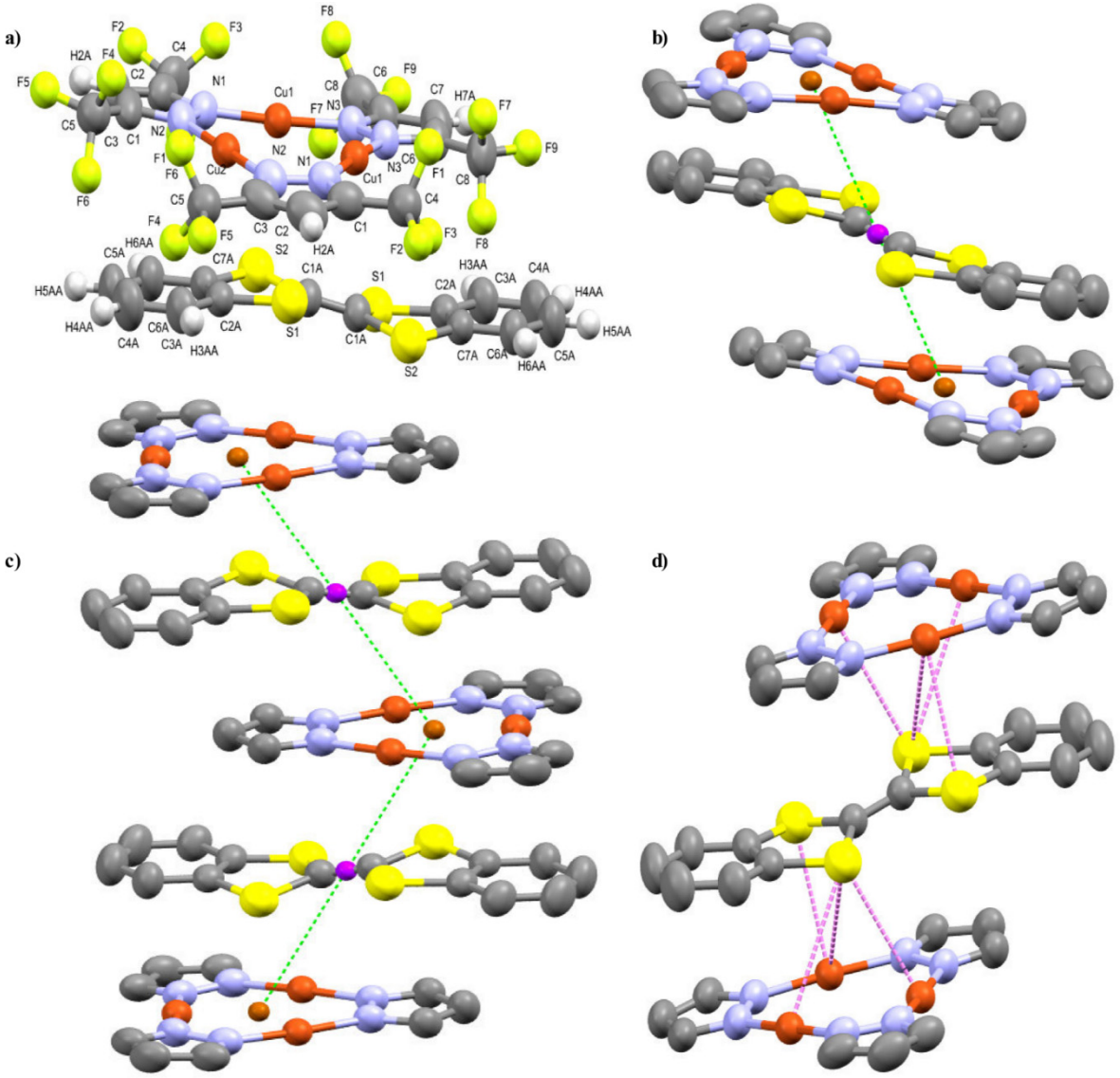

Figure 1. X-ray crystal structure for {[Cu(μ-3,5-$(CF_3)_2$pz)]$_3$DBTTF}, **1** (a) view of the charge-transfer complex in the solid-state structure together with the atom numbering scheme, (b) the contents of the unit cell illustrating interactions involving the calculated centroids for donor (Magenta) and acceptor (Maroon) molecules. Centroid···centroid contact is 4.174(1) Å, (c) one-dimensional crystal packing motif, and (d) the contents of the unit cell with the emphasis on Cu···S contacts (violet dotted lines) shorter than 4.0 Å. -CF_3 group and hydrogen atoms are omitted for the sake of clarity.

Structure of {[Ag(μ-3,5-(CF$_3$)$_2$pz)]$_3$DBTTF}, 2. Crystal structure of the charge transfer complex {[Ag(μ-3,5-(CF$_3$)$_2$pz)]$_3$DBTTF}, **2**, displays that complex **2** crystalizes in the monoclinic crystal system with *C2/c* space group. Single molecule of complex **2** in unit cell is depicted in **Figure 2 (a)**. The DBTTF donor molecule and the cyclic trimetallic Ag(I) complex are stacked in an integrated pattern above and below each other, which allows for enhanced orbital overlap as in complex **1.**

The acceptor molecules are centered toward the sulfur atoms and the donor and acceptor molecules form a zig-zag extended chain in crystal packing. There are four Ag···S contacts above and below each donor molecule interacting with acceptor molecule which are less than 4.0 Å as shown in **Figure 2 (d)**. The significant Ag···S interactions are 3.295(1) Å, 3.413(1) Å, 3.732(1) Å and 3.767(1) Å are shorter than those found for the Cu(I) and Au(I) analogue. The illustration of the calculated centroid-centroid interactions is given in **Figure 2 (b)**. The centroid-centroid interactions shows tightly bonded adjacent molecules for Ag(I)-based acceptor when compare to the Cu(I) and Au(I) acceptor molecules. This is obviously due to the strong acidic behavior of cyclic trimetallic Ag(I) complex compared to other coinage metal(I) complexes of same ligand as described previously.[30] Crystal packing motif that shows an infinite zig-zag chain of the donor-acceptor stack for complex **2**, is given in **Figure 2 (c)**.

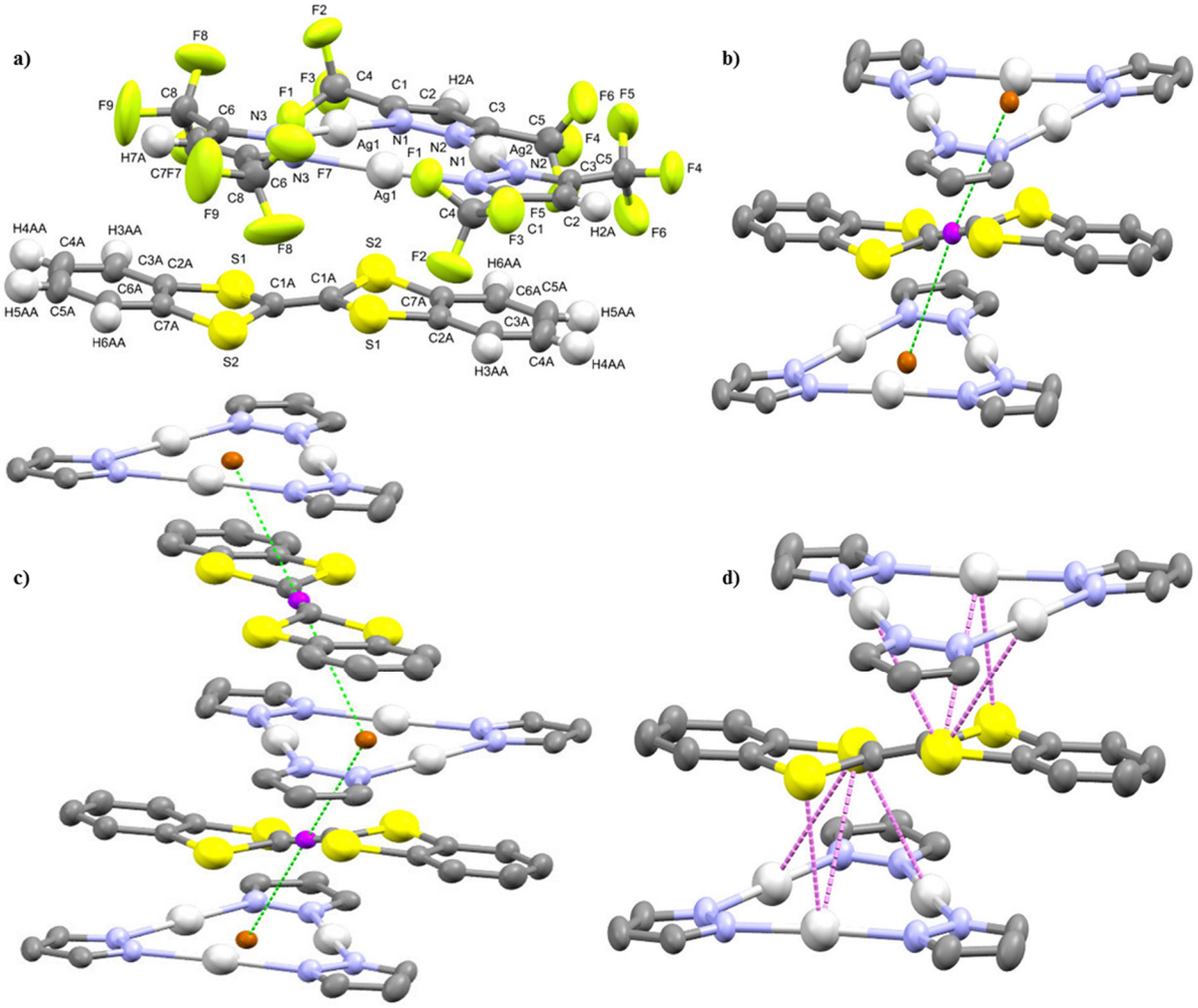

Figure 2. X-ray crystal structure for {[Ag(μ-3,5-$(CF_3)_2$pz)]$_3$DBTTF}, **2** (a) view of the charge-transfer complex in the solid-state structure together with the atom numbering scheme, (b) the contents of the unit cell illustrating interactions involving the calculated centroids for donor (Magenta) and acceptor (Maroon) molecules. Centroid···centroid contact is 4.134(1) Å, (c) one-dimensional crystal packing motif, and (d) the contents of the unit cell with the emphasis on Ag···S contacts (violet dotted lines) shorter than 4.0 Å. -CF_3 group and hydrogen atoms are omitted for the sake of clarity.

The orientation of the DBTTF molecules are in two different crystallographic spaces as in complex **1**, where the next neighboring DBTTF molecule in the stacks is always nearly

perpendicular to each other throughout the extended structures as shown in **Figure 2 (c)**. The integrated D-A-D-A supramolecular stacks shows convincing evidence of the charge transfer properties and other related conducting behavior which is also substantiated by the spectroscopic as well as computational studies described in sections below.

Structure of {[Au(μ-3,5-(CF$_3$)$_2$pz)]$_3$DBTTF}, 3. Charge transfer complex {[Au(μ-3,5-(CF$_3$)$_2$pz)]$_3$DBTTF}, **3**, crystalizes in the monoclinic space group *C2/c* with one molecule in the unit cell, the structure as shown in **Figure 3 (a)**, together with the atom numbering scheme. The DBTTF donor molecule and the cyclic trimetallic Au(I) complex are stacked in an integrated pattern above and below each other which allows for enhanced orbital overlap as in complexes **1** and **2**.

The acceptor molecules are centered toward the sulfur atoms of the donor molecules resulting in a zig-zag extended packing motif. Even though, our previous study indicated that Au(I) complexes are the least acidic among the similar derivatives of cyclic trimetallic monovalent coinage metal(I), there are still four Au···S contacts above and below each donor molecule as in the case of Ag(I) and Cu(I) complexes. The significant interaction of less than 4.0 Å between the cyclic trimetallic Au(I) acceptor molecule and donor molecules is shown in **Figure 3 (d)**. These significant Au···S interactions are 3.594(1) Å, 3.698(1) Å, 3.849(1) Å and 3.854(1) Å. However, donor-acceptor interaction in complex **3** is the weakest among cyclic trimetallic monovalent coinage metal(I) complexes with the same ligand.

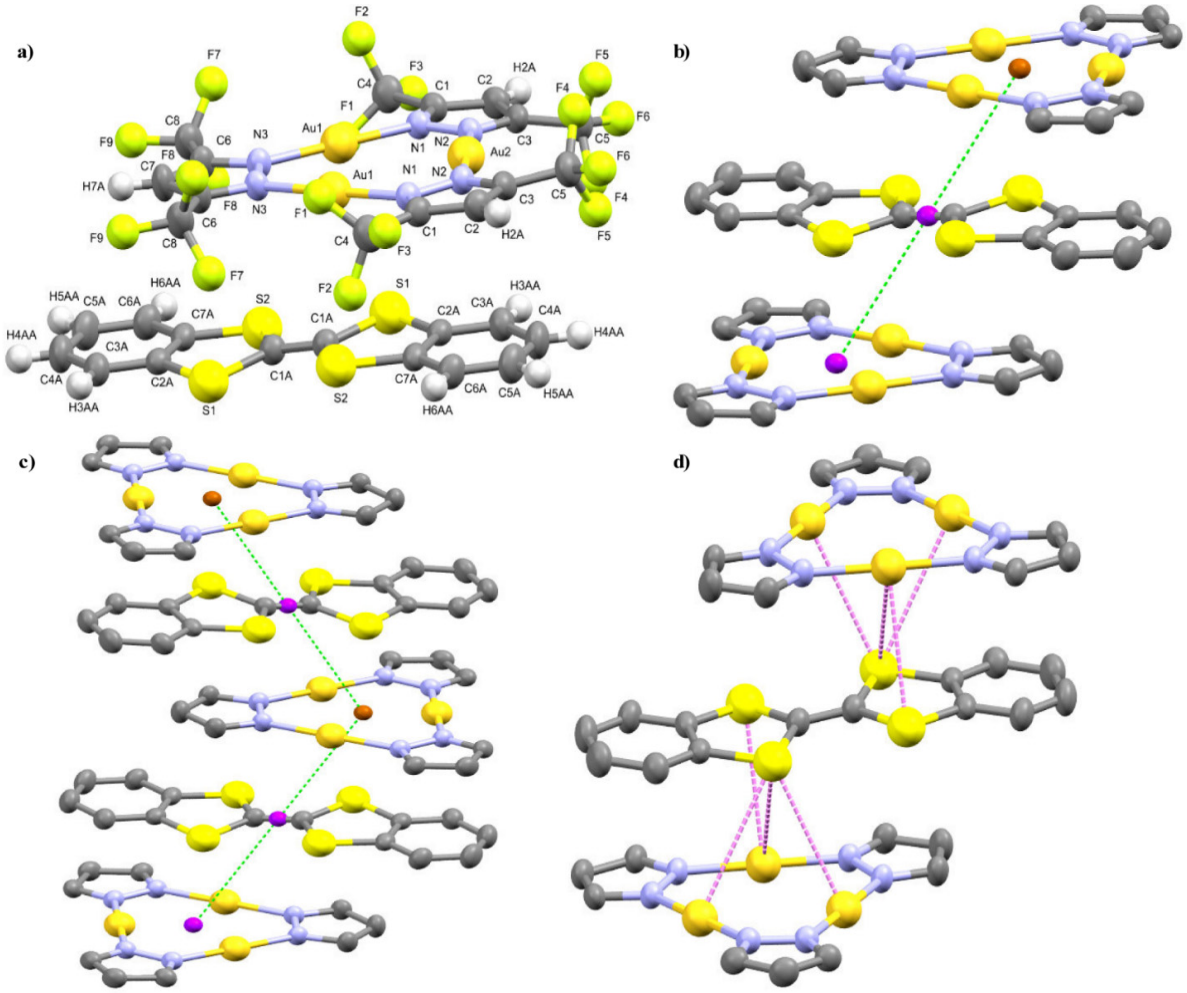

Figure 3. X-ray crystal structure for {[Au(μ-3,5-$(CF_3)_2$pz)]$_3$DBTTF}, **3** (a) view of the charge-transfer complex in the solid-state structure together with the atom numbering scheme, (b) the contents of the unit cell illustrating interactions involving the calculated centroids for donor (Magenta) and acceptor (Maroon) molecules. Centroid···centroid contact is 4.219(1) Å, (c) one-dimensional crystal packing motif, and (d) the contents of the unit cell with the emphasis on Au···S contacts (violet dotted lines) shorter than 4.0 Å. -CF_3 group and hydrogen atoms are omitted for the sake of clarity.

The illustration of the calculated centroid···centroid interactions is given in **Figure 3 (b)** and is also weaker compared to the Cu(I) and Ag(I) analogs, because the cyclic trimetallic Au(I) complex of the same ligands is the most basic compared to the same for other coinage metal(I) complexes. The complex **3** forms an infinite zig-zag chain of the donor-acceptor stack as shown in **Figure 3 (c)**. The orientation of the DBTTF molecules are in two different crystallographic space as in complex **1** and **2**, where the next neighboring DBTTF molecules in the stacks, are always nearly perpendicular to each other throughout the extended structures as shown in **Figure 3 (c)**.

Structure of {[Cu(μ-3,5-(CF$_3$)$_2$pz)]$_3$TTF}, 4. The crystal structure for the charge transfer complex {[Cu(μ-3,5-(CF$_3$)$_2$pz)]$_3$TTF}, **4**, on the other hand, reveals that complex **4** crystalizes in the monoclinic space group *C2/c* with one molecule in the unit cell, the structure as shown in **Figure 4 (a)**, together with the atom numbering scheme. The TTF donor molecule as DBTTF also forms the integrated stacks with the cyclic trimetallic Cu(I) complex that mediated by Cu···S above and below each other, allowing enhanced orbital-overlap than in DBTTF.

The acceptor molecules are centered toward the sulfur atoms of the donor molecules. However, the TTF molecules are arranged in 3-D spaces of solid-state crystal packing and results fascinating stacks that look like the single-stranded helical shape in crystal packing. These helical extended chains are composed of alternatively corner sharing TTF molecules, which are linked by strong Cu···S interactions. There are several Cu···S contacts above and below each donor molecule interacting with acceptor molecule, which are less than 4.0 Å as shown in **Figure 4 (d)**. The significant Cu···S interactions are 3.211(3) Å, 3.322(2) Å, 3.423(2) Å, 3.454(3) Å, 3.547(3) Å, 3.636(4), 3.661(4) Å, 3.841(2) Å and 3.925(2) Å. The illustration of the calculated

centroid···centroid interactions is given in **Figure 4 (b)** that are very strong compared to the DBTTF analog**.**

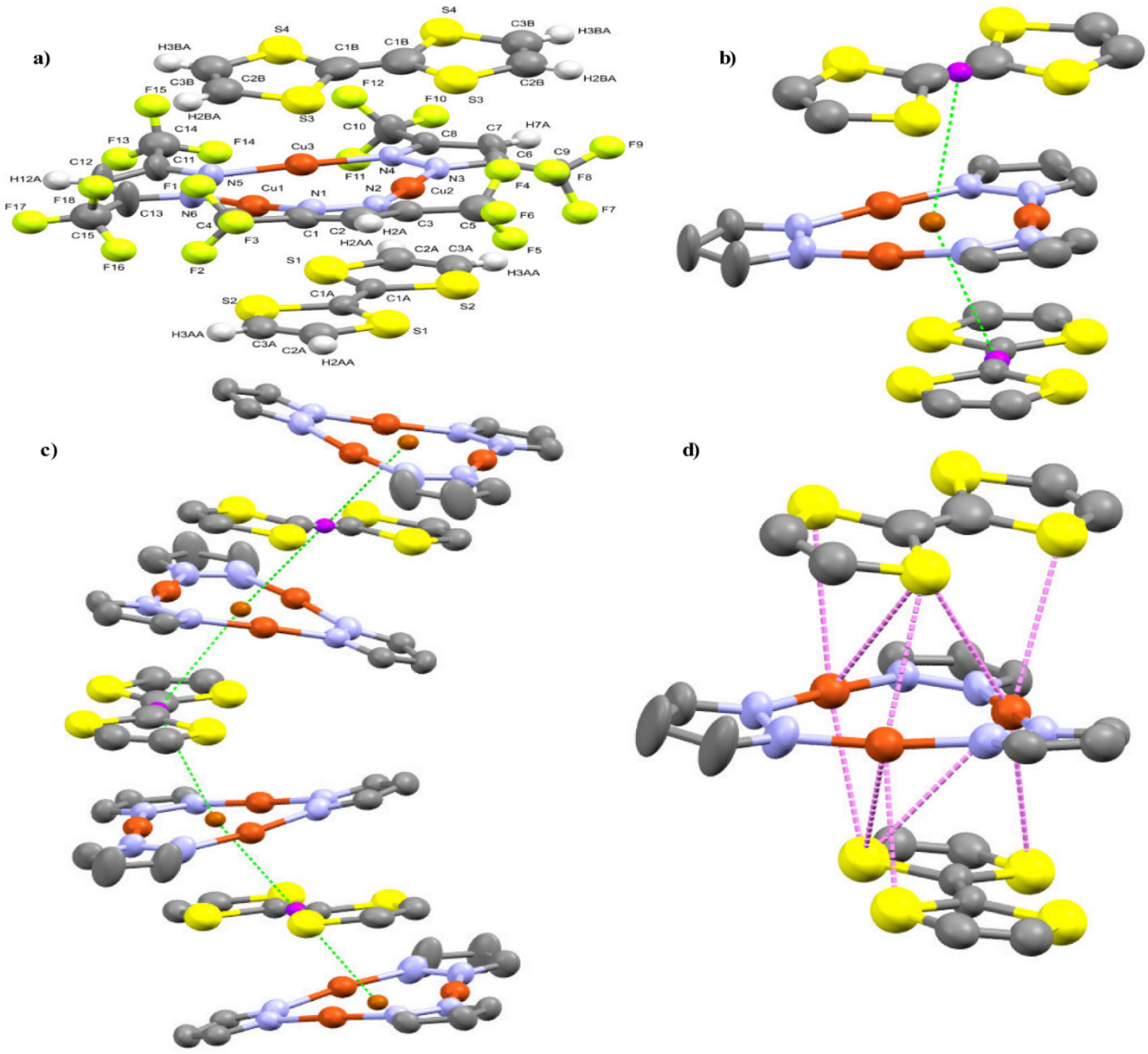

Figure 4. X-ray crystal structure for {[Cu(μ-3,5-$(CF_3)_2$pz)]$_3$TTF}, **4** (a) view of the charge-transfer complex in the solid-state structure together with the atom numbering scheme, (b) The contents of the unit cell illustrating interactions involving the calculated centroids for donor (Magenta) and acceptor (Maroon) molecules. Centroid···centroid contacts are 3.638(4) Å and

3.755(4) Å, (c) one-dimensional crystal packing motif, and (d) the contents of the unit cell with the emphasis on Cu···S contacts (violet dotted lines) shorter than 4.0 Å. -CF_3 group and hydrogen atoms are omitted for the sake of clarity.

The complex **4** forms infinite extended donor-acceptor stack which is shown in **Figure 4 (c)**. TTF molecules can be found in three different orientations in crystallographic axis and are always nearly perpendicular among each other throughout the extended structures as shown in **Figure 4** (**c**). The interaction of {[Cu(μ-3,5-$(CF_3)_2$pz)]$_3$ with TTF is stronger than those found with DBTTF.

Structure of {[Ag(μ-3,5-$(CF_3)_2$pz)]$_3$TTF}, 5. Single crystal structural determination analysis for the charge transfer complex {[Ag(μ-3,5-$(CF_3)_2$pz)]$_3$TTF}, **5**, shows that this complex crystalizes in the triclinic space group *P-1* with one acceptor molecule in a general position and two donors in a special position ((inversion center) in the asymmetric unit, the structure of which is depicted in **Figure 5 (a)**, together with the atom numbering scheme. TTF donor molecule and the cyclic trimetallic Ag(I) complex forms integrated pattern above and below each other, allowing greater orbital overlap than in DBTTF analogue. This might be due to the steric bulkiness of DBTTF *vs* TTF donor molecule.

The individual molecules of cyclic trimetallic Ag(I) complexes are centered towards the sulfur atoms of the TTF molecules to give rise a zig-zag extended chain crystal packing motif. There are four Ag···S contacts above and below each donor molecule interacting with acceptor molecule which are less than 4.0 Å as shown in **Figure 5 (d)**. The significant Ag···S interactions are 3.265(2) Å, 3.353(2) Å, 3.453(2) Å, 3.471(2) Å, 3.508(2) Å, 3.571(2) Å, 3.624(2) Å, 3.792(2) Å, 3.828(2) Å and 3.931(2) Å. The calculated centroid···centroid distances are shown in **Figure 5**

(b) and the infinite zig-zag extended chain mediated by Ag···S contacts of donor-acceptor molecules of complex **5**, is demonstrated in **Figure 5 (c)**. The positioning of the TTF molecules are in two different crystallographic axes, whereby, the next neighboring TTF molecule in the stacks is always perpendicular to one another throughout the extended structures as shown in **Figure (c)**.

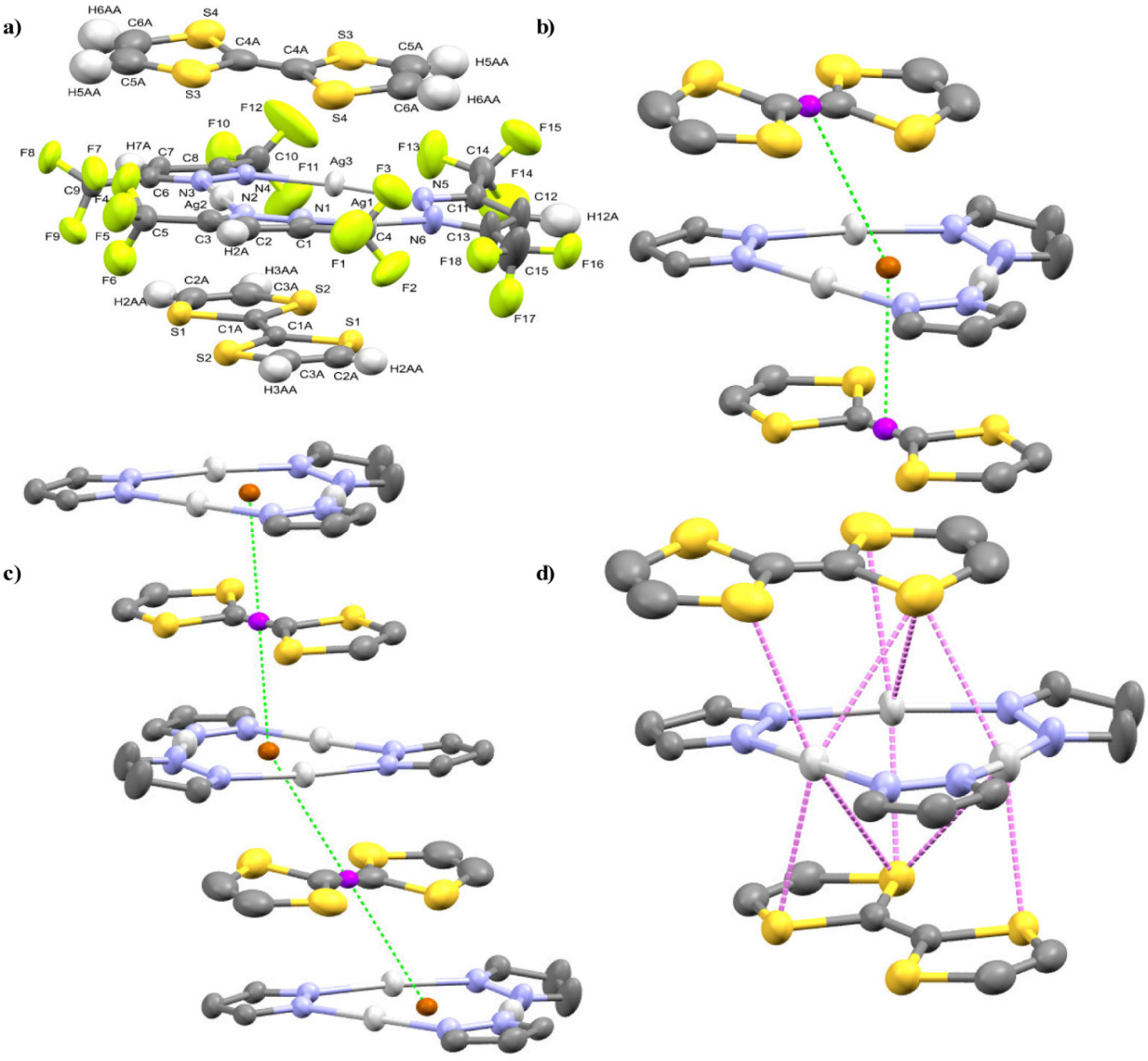

Figure 5. X-ray crystal structure for {[Ag(μ-3,5-$(CF_3)_2$pz)]$_3$TTF}, **5** (a) view of the charge-transfer complex in the solid-state structure together with the atom numbering scheme, (b) the contents of the unit cell illustrating interactions involving the calculated centroids for donor (Magenta) and acceptor (Maroon) molecules. Centroid···centroid contacts are 3.376(2) Å, 3.550(2) Å and 3.951(2) Å, (c) One-dimensional crystal packing motif, and (d) the contents of the unit cell with the emphasis on Ag···S contacts (violet dotted lines) shorter than 4.0 Å. -CF_3 group and hydrogen atoms are omitted for the sake of clarity.

Structure of {[Ag(μ-3,5-$(CF_3)_2$pz)]$_3$BEDT-TTF}, 8. Likewise, the solid-state crystal structure of charge transfer complex {[Ag(μ-3,5-$(CF_3)_2$pz)]$_3$BEDT-TTF}, **8**, crystalizes in the monoclinic space group *P21/n* with one molecule in the unit cell. The structure is shown in **Figure S1** (**a**) of supporting information together with the atom numbering scheme.

The BEDT-TTF donor molecule and the cyclic trimetallic Ag(I) complex are arranged in an integrated arrangement above and below each other, which allows enhanced orbital overlap. The acceptor molecules are attracted toward the sulfur atoms of the donor molecule, making a zig-zag extended chain crystal packing motif for complex **8**. There are several Ag···S contacts less than 4.0 Å above and below each of the donor molecule interacting with acceptor molecule, which are shown in **Figure S1** (**d**) of supporting information. The Ag···S interactions of 3.163(2) Å, 3.303(2) Å, 3.320(2) Å, 3.346(2) Å, 3.357(2) Å, 3.412(2) Å, 3.513(2) Å, 3.603(2) Å, 3.751(2) Å and 3.819(2) Å are were below the attractive d-π contacts of 3.750 Å. Calculated centroids of donor and acceptor molecules interacting to each other are depicted in **Figure S1** (**b**) of supporting information for illustration purposes.

The complex **8** forms infinite zig-zag extended chain of the donor-acceptor stack as shown in **Figure S1** (**c**) of supporting information. The orientation of the BEDT-TTF molecules are in two different crystallographic axes where the next neighboring BEDT-TTF molecules in the stacks are always nearly perpendicular to each other throughout the extended structures as shown in **Figure S1** (**c**) of supporting information.

Spectroscopic Studies

A. ***Nuclear Magnetic Resonance (NMR).*** The behavior of binary adduct **1** in solution was investigated by NMR chemical shift measurements and $^{19}F,^{1}H$ HOESY NMR, taking advantage from the presence of highly sensitive ^{1}H and ^{19}F nuclei in the interacting moieties. $^{19}F,^{1}H$ HOESY NMR experiments[31] allow the spatial arrangement of the interacting moieties in solution to be directly determined. $^{19}F,^{1}H$ HOESY NMR has been already successfully applied to investigate the intermolecular structure of ion pairs,[32] ionic liquids,[33] frustrated Lewis pairs,[34] host-guest assembly,[35] and of supramolecular adducts held together by acid-base interaction,[36] hydrogen bonding,[37] and halogen bonding[38] interactions.

The room temperature ^{1}H NMR spectrum of a freshly prepared saturated solution of **1** in CD_2Cl_2 (ca. 8 mM) consists of a broad resonance at δ_H = 7.16 ppm and a sharper one at δ_H = 6.99 ppm. The latter is assigned to H4 protons of $[Cu(\mu\text{-}3,5(CF_3)_2pz)]_3$, owing to the presence of its strong NOE contact with CF_3 groups [$\delta_F(CF_3)$ = -60.95 ppm] in the $^{19}F,^{1}H$ HOESY NMR spectrum; the resonance at 7.16 ppm is assigned to the aromatic protons of DBTTF. A comparison with NMR chemical shifts of pure $[Cu(\mu\text{-}3,5(CF_3)_2pz)]_3$ indicates that both H4 and CF_3 moieties are significantly shifted {δ_H(H4) = 7.071 ppm and $\delta_F(CF_3)$ = -61.04 ppm in free $[Cu(\mu\text{-}3,5(CF_3)_2pz)]_3$,

respectively}, supporting the presence of a certain amount of **1** in solution in equilibrium with free $[Cu(\mu\text{-}3,5(CF_3)_2pz)]_3$ and DBTTF. Consistently, the broad resonance due to the aromatic protons of DBTTF is also shifted with respect to those of pure DBTTF [δ_H(Ha) = 7.29 ppm, δ_H(Hb) = 7.15 ppm]. However, no intermolecular cross peaks were detected in the $^{19}F,^{1}H$ HOESY NMR spectra, acquired under different experimental conditions. This can due to the fast relaxation of aromatic protons of DBTTF or to the fact that the amount of **1** in solution is rather small. For these reasons, adduct **1** was studied in cyclohexane, a solvent more inert and with a substantially lower polarity than methylene chloride, where the formation of **1** intermolecular adducts was expected to be favored. This was indeed the case. Adding increasing amounts of solid $[Cu(\mu\text{-}3,5(CF_3)_2pz)]_3$ to a 0.8 mM solution of DBTTF in C_6D_{12} resulted in the progressive shift of DBTTF ^{1}H NMR resonances toward lower frequencies (**Figure 6**); the resonance due to Ha protons is more affected than that due to Hb protons (as observed in CD_2Cl_2). Clearly, both the ^{1}H and ^{19}F NMR resonances of $[Cu(\mu\text{-}3,5(CF_3)_2pz)]_3$ gradually shift toward that of free $[Cu(\mu\text{-}3,5(CF_3)_2pz)]_3$ as its relative concentration increases (**Figure 6**). Qualitatively, these observations confirm the formation of **1** in solution and indicate that **1** equilibrates with free components at a rate that is fast on the chemical shift NMR time scale, i.e. the observed chemical shifts are weight-averages of those corresponding to **1** and its components. Although full quantitative analysis by chemical shift titration methods is hampered by the precipitation of **1** as the concentration of $[Cu(\mu\text{-}3,5(CF_3)_2pz)]_3$ increases (**Figure 6**, spectra f and g), an estimate of the equilibrium association constant (K_{assoc}) can be obtained by analyzing the data in the low concentration regime, where the system remains fully soluble. K_{assoc} was estimated by applying the method described by Dougherty[39] under the assumptions that *i*) the limiting ^{19}F NMR chemical shift of $[Cu(\mu\text{-}3,5(CF_3)_2pz)]_3$ unit in adduct **1** is similar to that experimentally observed for the solution with the highest DBTTF/Cu molar ratio

(0.8mM/0.08mM, **Figure 6** spectrum b) and *ii*) DBTTF and $[Cu(\mu\text{-}3,5(CF_3)_2pz)]_3$ form a 1:1 adduct. It was found that K_{assoc} amounts to: $7.9x10^3$ M^{-1}, $7.0x10^3$ M^{-1} and $7.0x10^3$ M^{-1} for solutions containing 0.27 mM, 0.44 mM and 0.62 mM of $[Cu(\mu\text{-}3,5(CF_3)_2pz)]_3$, respectively, at constant DBTTF analytical concentration (0.8 mM) (**Figure 6**, spectra c, d and e). Such values are reasonable and consistent with those determined for neutral species in C_6D_{12} that associate through weak forces.[40]

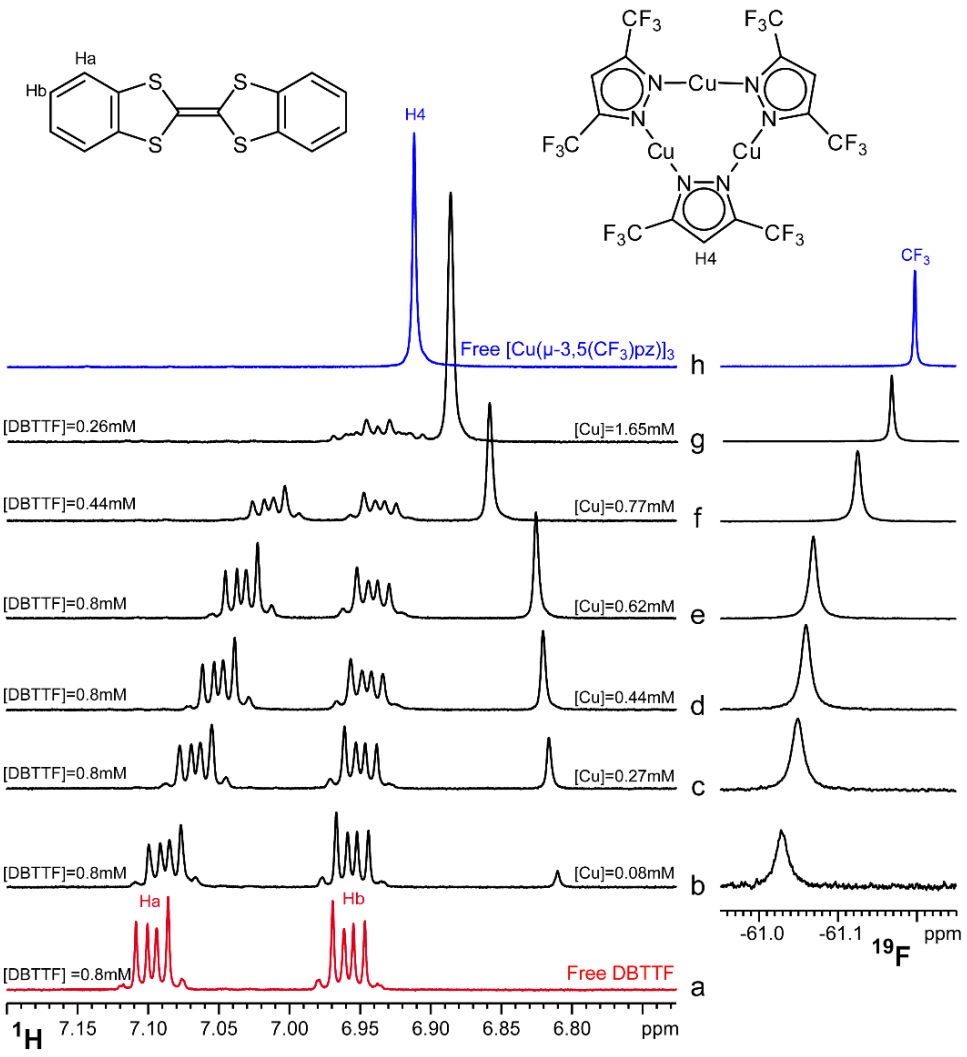

Figure 6. Sections of the ^1H (left) and ^{19}F (right) NMR spectra recorded after consecutive additions of solid $[Cu(\mu\text{-}3,5(CF_3)_2pz)]_3$ to a 0.8 mM solution of DBTTF in C_6D_{12}.

The supramolecular structure of **1** in solution was determined by 1D $^{1}H,^{19}F$ HOESY NMR measurements.[41a]The latter were carried out at 333 K for a solution containing an excess of DBTTF {DBTTF = 7.8 mM, $[Cu(\mu\text{-}3,5(CF_3)_2pz)]_3$ = 3.00 mM} in order to maximize the amount of **1** in solution. As shown in **Figure 7**, intermolecular NOEs are observed between the CF_3 moiety of $[Cu(\mu\text{-}3,5(CF_3)_2pz)]_3$ and aromatic protons of DBTTF, directly confirming the presence of adduct **1** in solution. Integration indicates that CF_3-H_a HOE contact is about 2.44 times stronger than the corresponding CF_3-H_b one. Since the NOE intensity in proportional to the six-inverse power of internuclear distance,[41b] the average CF_3-H_b intermolecular distance in solution is about 1.16 times longer than the average CF_3-H_a intermolecular distance. In nice agreement, the average CF_3-H_b and CF_3-H_a distances computed from the solid-state structure of **1** (**Figure 1a**) are 5.27 Å and 4.46 Å, respectively, whose ratio is 1.18. Consequently, it appears that the preferred relative orientation in solution of the two interacting moieties of adduct **1** must be very similar to that observed in the solid state.

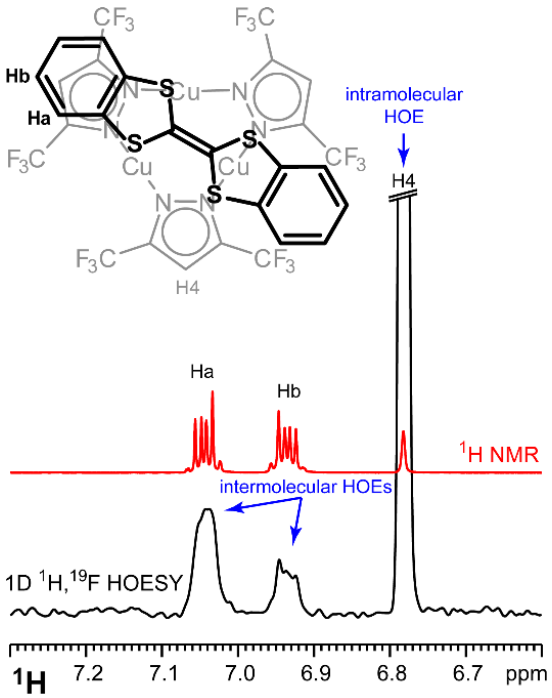

Figure 7. ^{1}H (top) and 1D ^{1}H, ^{19}F HOESY (bottom) NMR spectra of a solution containing DBTTF (7.8 mM) and $[Cu(\mu\text{-}3,5(CF_3)_2pz)]_3$ (3.00 mM) (333 K, C_6D_{12}), showing that intermolecular CF_3-H_a contact is stronger than CF_3-H_b one.

B. Fourier Transfer Infrared (FTIR). Vibrational spectroscopic study for the solid samples of the charge transfer complexes has performed and the representative mid-IR spectra for $\{Cu[\mu\text{-}3,5(CF_3)_2pz]\}_3$ acceptor complex, charge transfer complex $\{Cu[\mu\text{-}3,5(CF_3)_2pz]_3DBTTF\}$ and DBTTF donor molecule are shown in **Figure S2** of supporting information.

All the results are summarized in **Table S1** that contain the C4-H mid- IR stretching frequencies in acceptors and C=C-H Mid-IR stretching frequencies in donors. Overall, the C4-H Mid-IR stretching frequencies in acceptors slightly decrease while C=C-H mid- IR stretching frequencies in donors remain the same or slightly increase as the indication of the formation of charge transfer complexes.

C. UV-Vis-NIR Absorption and Diffuse Reflectance (DR) Studies. The most promising evidence to validate the formation of the charge transfer complexes described herein, comes from the physical color associated with them and the formation of colored solutions and solids such as: yellow (binary donor-acceptor adducts **1-6**), and bright orange (binary donor-acceptor adducts **7-9**) upon mixing the colorless acceptor molecules - cyclic trimetallic coinage metal(I) complexes $[Cu(\mu\text{-}3,5\text{-}(CF_3)_2pz)]_3$, $[Ag(\mu\text{-}3,5\text{-}(CF_3)_2pz)]_3$, and $[Au(\mu\text{-}3,5\text{-}(CF_3)_2pz)]_3$ with pale yellow (TTF and DBTTF) and orange (BEDT-TTF) organic donor molecules accompanied our findings herein. Further investigations by solution and solid-state electronic absorption studies supplements these

results. Relevant absorption data of dichloromethane solutions and the solid sample of the binary donor-acceptor adducts are illustrated in **Figures 8,S3-S10** and in **Table S2**.

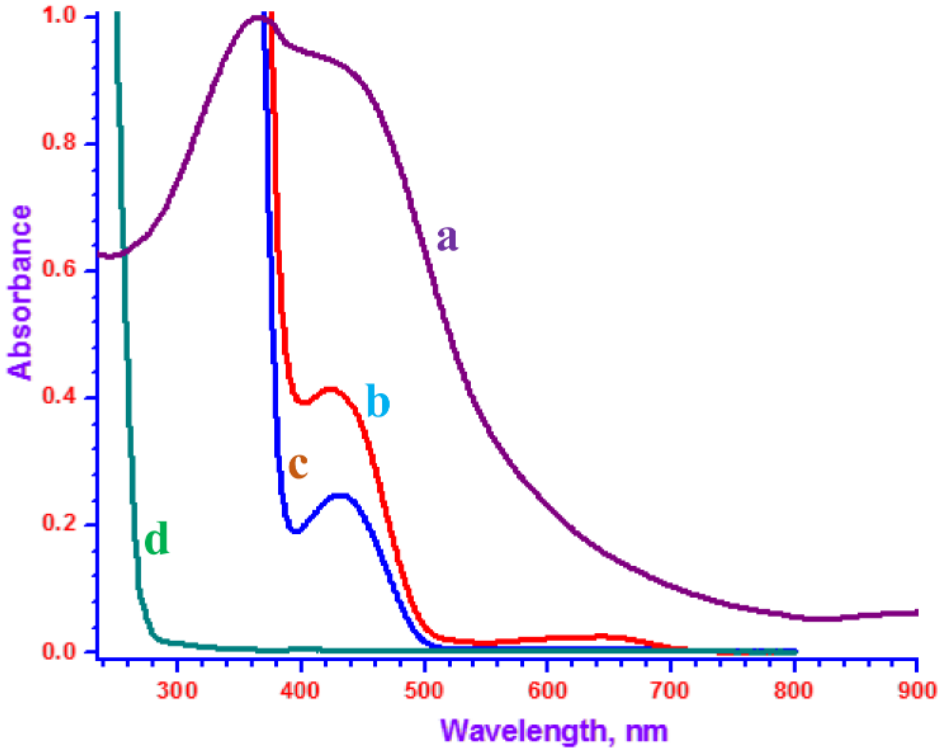

Figure 8. Electronic spectral data for (a) solid sample of charge transfer binary donor-acceptor adduct, {[Ag(μ-3,5-$(CF_3)_2$pz)]$_3$DBTTF}, **2**, (b) 1 mM dichloromethane solution of {[Ag(μ-3,5-$(CF_3)_2$pz)]$_3$DBTTF}, **2**, (c) 1 mM dichloromethane solution of donor (DBTTF) alone, and (d) 1 mM dichloromethane solution of acceptor [Ag(μ-3,5-$(CF_3)_2$pz)]$_3$ alone.

The representative electronic spectral data as shown in **Figure 8** compares the absorption spectra of 1 mM dichloromethane solutions of the [Ag(μ-3,5-$(CF_3)_2$pz)]$_3$ acceptor alone, DBTTF donor alone, the charge transfer binary donor-acceptor adduct {[Ag(μ-3,5-$(CF_3)_2$pz)]$_3$DBTTF}, **2** and its solid-state diffuse reflectance spectral data. The electronic spectrum shown in **Figure 8** (**b**) for the 1 mM dichloromethane solution of binary donor-acceptor adduct **2** reveals strong

absorption bands that extend the spectroscopic response towards longer wavelength if compared with the electronic spectrum (**c**) for the DBTTF donor alone and the electronic spectrum (**d**) for [Ag(μ-3,5-$(CF_3)_2$pz)]$_3$ acceptor alone. The distinct absorption shoulder that can be seen in the electronic spectrum (**b**) centered at ~650 nm is most probably due to the strong donor-acceptor charge transfer (DACT) interactions between the DBTTF donor and [Ag(μ-3,5-$(CF_3)_2$pz)]$_3$ acceptor molecules. The diffuse reflectance data reveals the strong absorption tendency of charge transfer binary donor-acceptor adduct, **2**, in the solid state and is readily seen as the dominant absorption band as demonstrated in the spectrum (**a**). The electronic absorption spectra shown in **Figures S3** and **S4** for charge transfer binary donor-acceptor adducts **1** and **3**, respectively, also have similar electronic absorption profile to that for **2** discussed herein. Likewise, the electronic absorption spectral data for binary donor-acceptor adducts {[Cu(μ-3,5-$(CF_3)_2$pz)]$_3$TTF}, **4,** {[Ag(μ-3,5-$(CF_3)_2$pz)]$_3$TTF}, **5**, and {[Au(μ-3,5-$(CF_3)_2$pz)]$_3$TTF}, **6** are shown in **Figures S5-S7** that extend the spectroscopic response towards longer wavelength when compared with the electronic spectra for TTF-donor and acceptors alone. Additionally, **Figures S8-S10** compare the electronic absorption spectra of solutions and solid sample of {[Cu(μ-3,5-$(CF_3)_2$pz)]$_3$BEDT-TTF}, **7**, {[Ag(μ-3,5-$(CF_3)_2$pz)]$_3$BEDT-TTF}, **8**, and {[Au(μ-3,5-$(CF_3)_2$pz)]$_3$BEDT-TTF}, **9** with the respective acceptor alone and with the BEDT-TTF donor alone, showing that the absorption towards longer wavelength, as the indication of the DACT interactions, exist between the donor (BEDT-TTF) and the acceptor molecules.

Lastly, the solids and the solutions of the charge transfer binary donor-acceptor adducts described herein, do not display any visible photoluminescence emission at both room as well as cryogenic temperatures, even though the cyclic trinuclear monovalent coinage metal complexes of pyrazolate and imidazolate including [Cu(μ-3,5-$(CF_3)_2$pz)]$_3$ and [Au(μ-3,5-$(CF_3)_2$pz)]$_3$ are well-

known complexes for their brightly phosphorescent properties.[12, 42] This is not surprising, since the luminescence of azolated cyclic trimetallic complexes of monovalent coinage metals is often related to the metallophilic interactions, which have been disrupted in the charge transfer complexes.[12c]

D. Computational Studies. Three kinds of computations have been performed at different sophistication levels of the molecular/supramolecular model and theory. First are qualitative molecular DFT single-point computations at the crystallographic geometry for the donor/acceptor model of donor-acceptor binary adduct **4** to show the Kohn-Sham contours of frontier orbitals. Thus, **Figure 9** shows that the four highest occupied molecular orbitals (HOMO through HOMO-3) have the electron density localized on the TTF molecule, bearing out its donor character. In stark contrast, the four lowest unoccupied molecular orbitals (LUMO through LUMO-3) have the electron density localized on the $\{[Cu(\mu\text{-}3,5\text{-}(CF_3)_2pz)]_3$ molecule, bearing out its acceptor character. Calculations were also performed for the cation and anion to ascertain that the singly occupied molecular orbital (SOMO) remains characteristic of the donor and acceptor molecule, respectively, hence safeguarding against Koopmans' Theorem considerations.

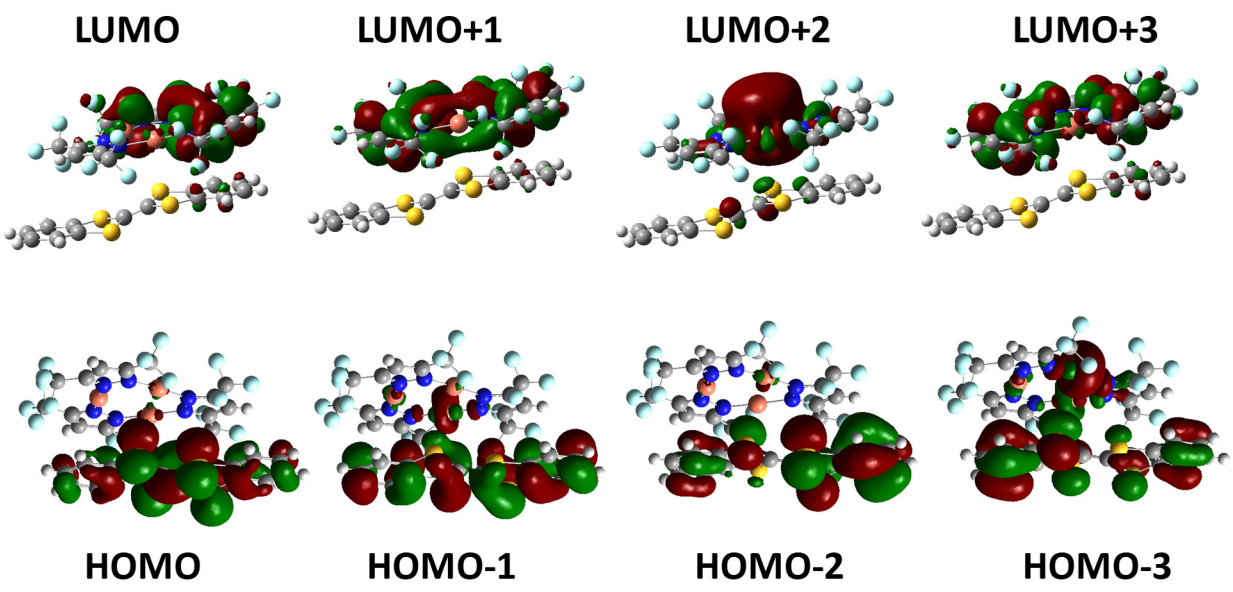

Figure 9. Kohn-Sham orbital contours of the frontier orbitals for compound **4** at its crystallographic geometry according to B3LYP/LANL2DZ calculations.

The second set of calculations aimed to predict the donor-acceptor optimized structure of donor-acceptor binary adduct **3**, giving rise to a reasonably good accuracy for a supramolecular interaction, as illustrated in **Table 3** and **Figure S12**. The TPSS/Def2-TZVP-D3 calculations have performed well because this level of theory including Grimme correlation,[29] which is suitable to describe dispersion forces that govern the donor-acceptor supramolecular interaction in {[Au(μ-3,5-$(CF_3)_2$pz)]$_3$DBTTF so as to give results in excellent agreement with the experimental structure. The optimized molecular structure of {[Au(μ-3,5-$(CF_3)_2$pz)]$_3$DBTTF} complex is shown in **Figure S12** while **Table 3** lists the relevant bond lengths; the short donor-acceptor contacts demonstrate good correlation with the experimental results in terms of separation between the donor and acceptor molecules in the donor-acceptor integrated stacks.

Table 3. Calculated bond lengths (Å) for {[Au(μ-3,5-$(CF_3)_2$pz)]$_3$DBTTF}, **3**, optimized with the TPSS/Def2-TZVP-D3. The bonds represented are the average intramolecular Au···Au aurophilic distance in the acceptor molecule, the two Au···C intermolecular distances between the acceptor and donor molecules, and the intramolecular C-S bond distance in the donor molecule.

	{[Au(μ-3,5-$(CF_3)_2$pz)]$_3$DBTTF}, **3**	
	TPSS/Def2-TZVP-D3	Experimental
Au···Au	3.405	3.339(2)
Au···C Au···C	3.793 3.660	3.698(2) 3.698(2)
C-S	1.764 1.753	1.754(3) 1.754(3)

The third set of calculations utilized the extended Hückel tight binding (EHTB) method on the entire crystal structure of the integrated stacks of the charge transfer complexes **3**, **4**, and **5**. The calculations for the solid-state crystal structures reveal their electronic structure and consequent conducting properties of binary donor-acceptor adducts of cyclic trimetallic coinage metal(I) complexes with organic ligand donors. The donor-acceptor extended chains in the solid state of these complexes are predicted to exhibit conducting behavior with a large contribution

from π and π* bands of TTF and DBTTF to the valence and conduction bands. **Figure 10A** shows a plot of the total EHTB density of states (DOS) for {[Au(μ-3,5-$(CF_3)_2$pz)]$_3$DBTTF}, **3**, giving rise to a Fermi level located at -9.50 eV. Also, the band gap zone seems to be continuous with the Fermi level crossing it. Therefore, {[Au(μ-3,5-$(CF_3)_2$pz)]$_3$DBTTF}, **3**, can be predicted as metallic material according to the EHTB calculations. Previous work[9b,9c] on other binary donor-acceptor materials done by some of the authors, however, has suggested that this is an overestimated Fermi level as other more advanced methods suggested a semiconducting character, instead a metallic. Our goal herein is to use the qualitative EHTB method simply to demonstrate the band structure distinction from molecular description as pertains to the electronic structure of these materials. For this purpose, the data shown in **Figures 10A-C** demonstrate an unmistakable character for the former band structure description (high DOS) instead of the latter molecular orbital description (discrete MO levels). In addition, **Figure 10** shows the total DOS and the DOS projections for gold and DBTTF contribution in the material {[Au(μ-3,5-$(CF_3)_2$pz)]$_3$DBTTF}, **3**, along with Au and DBTTF with a large delocalization in the valence-conduction band structures, thus indicating the role of the fragment {[Au(μ-3,5-$(CF_3)_2$pz)]$_3$ as acceptor, and DBTTF as a donor ligand. In Figure **10B**, we plot different projections: Au projection (middle), and DBTTF (right). The projections in shaded region, display the results for {[Au(μ-3,5-$(CF_3)_2$pz)]$_3$DBTTF}, **3**, in the valence band containing the Fermi level (left). **Figures 10A-C** show that the filled π-orbitals of the organic ligand pyrazolate lies below both the Au(I) *d*-orbitals and the DBTTF π-orbitals in the BV zone. The differences of π/π^* alone are lying at high energy according to the sulfur parameters. Also, a large dispersion of organic ligand was observed (right side in **Figure 10)** demonstrating the good donor – acceptor interaction character of this material.

Similarly, calculations for the solid-state crystal structures of the charge transfer complexes {[Cu(μ-3,5-$(CF_3)_2$pz)]$_3$TTF}, **4**, and {[Ag(μ-3,5-$(CF_3)_2$pz)]$_3$TTF}, **5**, were also performed with the extended Hückel tight binding (EHTB) methods to study their electronic band structure and consequent properties by analyzing the contribution of the metal in the ligand in the band structure.

Under EHTB calculations, both compounds present large metallic behavior (see the band continuity in the region croosed by the Fermi level (high electronic level) as shown in **Figures 10B** and **10C**). We observe then, the core metal projections contribution for Cu and Ag metals mixing with a large part of the organic ligand in the conduction band are different (see middle of **Figures 10B** and **10C**). Copper has greater influence on the band gap than silver has. Also, the lowest unoccupied bands are localized preferentially on the TTF (π^*) ligand in silver complexes displaying a larger acceptor-donor interactions vs the copper material (see the large band dispersion in the third box of **Figures 10B** and **10C**). Therefore, the analysis of DOS for the charge transfer complexes **3**, **4** and **5** shows a different contribution of the organic ligand and different DOS of materials in the band valence zone which presents different band structure and predicts that the three binary complexes show a metallic behavior that may be used in electronic devices related to such interesting electronic properties.

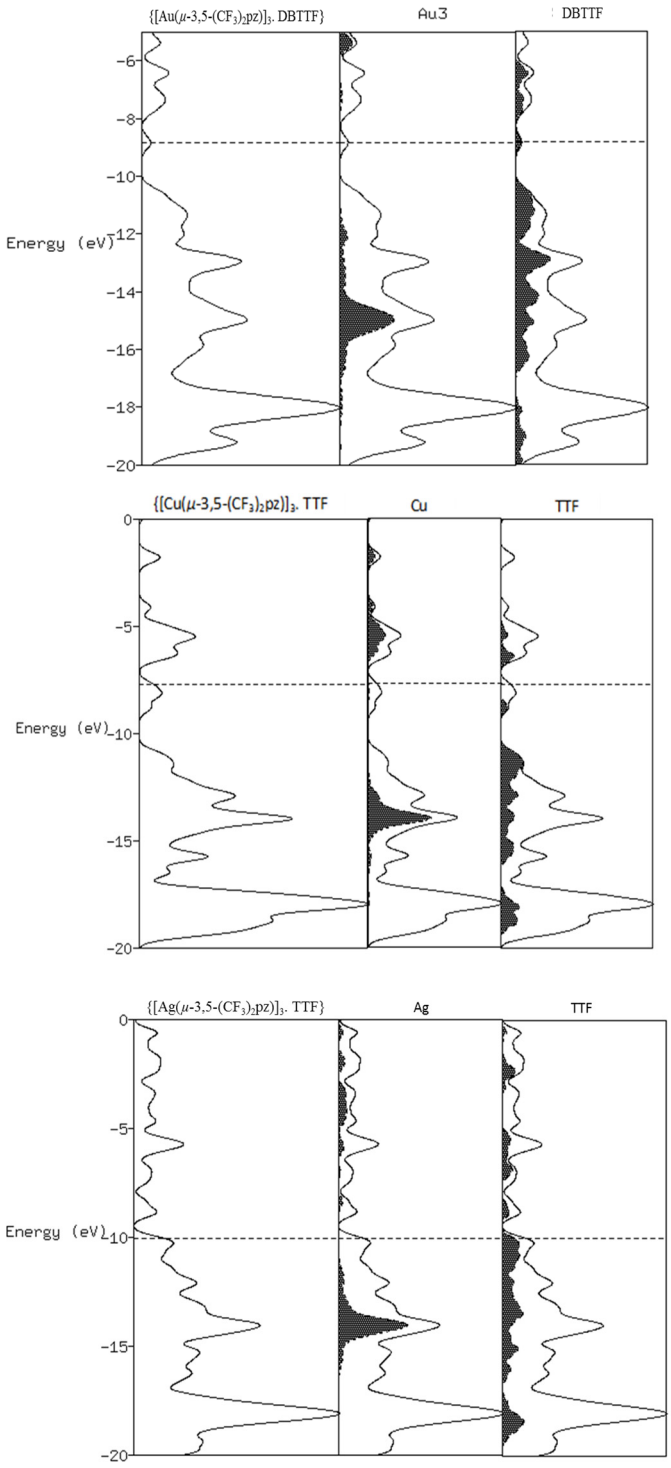

Figure 10. DOS plots for the crystal structure of **3** (top/**A**), **4** (middle/**B**) and **5** (bottom/**C**) showing the total DOS (left), the contribution of the acceptor molecule's metal core (shaded middle) and TTF/DBTTF donor molecule (shaded right). The dotted line corresponds to the Fermi level.

SUMMARY AND CONCLUSIONS

The comprehensive, both experimental and theoretical investigations of monovalent coinage metal-based donor-acceptor integrated stack as conducting functional materials are reported. The charge transfer complexes {[Cu(μ-3,5-$(CF_3)_2$pz)]$_3$DBTTF}, **1**, {[Ag(μ-3,5-$(CF_3)_2$pz)]$_3$DBTTF}, **2**, {[Au(μ-3,5-$(CF_3)_2$pz)]$_3$DBTTF}, **3**, {[Cu(μ-3,5-$(CF_3)_2$pz)]$_3$TTF}, **4**, {[Ag(μ-3,5-$(CF_3)_2$pz)]$_3$TTF}, **5**, {[Au(μ-3,5-$(CF_3)_2$pz)]$_3$TTF}, **6**, {[Cu-(μ-3,5-$(CF_3)_2$pz)]$_3$BEDT-TTF}, **7**, {[Ag(μ-3,5-$(CF_3)_2$pz)]$_3$BEDT-TTF}, **8**, and {[Au-(μ-3,5-$(CF_3)_2$pz)]$_3$BEDT-TTF}, **9** are prepared by reacting monovalent coinage metal complexes {[Cu(μ-3,5-$(CF_3)_2$pz)]$_3$, {[Ag(μ-3,5-$(CF_3)_2$pz)]$_3$, and {[Au(μ-3,5-$(CF_3)_2$pz)]$_3$ with organic donor molecules. Their solid-state single crystal structural properties and supramolecular chemistry have been analyzed toward their potential use in the molecular electronic devices. These materials exhibit properties such as close packing that maximizes the intermolecular overlap of the donor and acceptor units as the building blocks to form integrated stacks mediated by the *d*-π interactions. It is reasonable to assume that these binary donor-acceptor adducts form after a first π-π acid base interaction, leading to tight adducts depending on the acid base properties of both the acceptor trimer as well as the organic donor. Then, the fact we have 1 : 1 or 1 : 2 compounds is an issue related to this aspect, a kind of valence of the trimer based on its acid or basic strength. By the way, the NMR solution studies on adduct **5** support the fact that the formation of a 1 : 1 A/D adduct in solution may represent the first step of the reaction. As for the nature of the bonding in the binary, despite the fact that the DBTTF molecule exhibits stronger donor properties than TTF molecule, theoretical studies predict that the charge transfer complexes containing TTF and its derivatives are metallic. Hence, in TTF adducts with the cyclotrimers herein, we have likely metallic bonds leading us to unravel another important issue about the study of the nature of the chemical bonding for this class of

donor/acceptor binary adducts. The experimental and theoretical studies are underway in our labs for further investigation of the conducting properties and screening studies toward optoelectronic device fabrication[42c] and/or photocatalysis use.

ASSOCIATED CONTENT

Supporting Information

Crystal structures of binary donor-acceptor adducts **1-5** and **8** in CIF format; (also deposited at the Cambridge Crystallographic Data Centre as CCDC 1862609, 1862610, 1862611, 1862612, 1862613, and 1862614) and further supporting information are available free of charge on the ACS publications website at http://pubs.acs.org.

AUTHORS INFORMATION

Corresponding Authors

*E-mail: Omary@unt.edu (M. A. Omary)

*E-mail: rossana.galassi@unicam.it (R. Galassi)

Authors Contributions

The manuscript was written through contributions of all authors. All authors have given approval to the final version of the manuscript.

Notes

The authors declare no competing financial interest.

ACKNOWLEDGEMENTS

This research has been supported by Welch Foundation Grant B-1542 and NSF Grant CHE-1413641 to M.A.O. for research support and NSF Grant CHE-1726652 for equipment support; by FAR of University of Camerino and CIRCSMB to R.G.; and by 2019 Arnold Grant of Lebanon Valley College to M. M. G. Computational support to H.R. is acknowledged for the University of North Texas (under NSF Grant CHE-1531468), the Academy of Finland for providing access to their computational resources and Arab fund for their support. A.M. and C.Z. thank PRIN 2015 (20154X9ATP_004), University of Perugia and MIUR (AMIS,"Dipartimenti di Eccellenza - 2018-2022" program), for financial support.

REFERENCES

1. (a) Shaik, S. S. On the stability and properties of organic metals and their isomeric charge-transfer complexes. *J. Am. Chem. Soc.* **1982**, 104, 5328-5334. (b) Ferraris, J.; Cowan, D. O.; Walatka, V. V., Jr.; Perlstein, J. H. Electron transfer in a new highly conducting donor-acceptor complex. *J. Am. Chem. Soc.* **1973**, 95, 948. (c) Coleman, L. B.; Cohen, M. J.; Sandman, D. J.; Yamagashi, F. G.; Garito, A. F.; Heeger, A. J. Superconducting fluctuations and the peierls instability in an organic solid. *J. Solid State Commun.* **1973**, 12, 1125. (d) Wudl, F. From organic metals to superconductors: managing conduction electrons in organic solids. *Acc. Chem. Res.* **1984**, 17, 227. (e) Williams, J. M.; Ferraro, J. R.; Thorn, R. J.; Carlson, K. D.; Geiser, U.; Wang, H. H.; Kini, A. M.; Whangbo, M.-H. Organic Superconductors (including Fullerenes): Synthesis, structure, properties, and theory; Prentice Hall: Englewood Cliffs, NJ, **1992**.
2. (a) Bousseau, M.; Valade, L.; Legros, J.-P.; Cassoux, P.; Garbauskas, M.; Interrante, L. V. Highly conducting charge-transfer compounds of tetrathiafulvalene and transition metal-"dmit" complexes. *J. Am. Chem. Soc.* **1986**, 108, 1908. (b) Cassoux, P. Molecular (super) conductors derived from bis-dithiolate metal complexes. *Coord. Chem. Rev.,* **1999**, 185-186, 213-232. (c) Smucker, B. W.; Dunbar, K. R. Homoleptic complexes of Ag(I), Cu(I), Pd(II) and Pt(II) with tetrathiafulvalene-functionalized phosphine ligands. *Dalton Trans.* **2000**, 8, 1309. (d) Miyasaka, H.; Campos-Ferna´ndez, C. S.; Cle´rac, R.; Dunbar, K. R. A one-pot high-yield synthesis of a paramagnetic nickel square from divergent precursors by anion template assembly. *Angew. Chem., Int. Ed.* **2000**, 39, 3831. (e) Zhao, H.; Heintz, R. A.; Ouyang, X.; Dunbar, K. R. Spectroscopic, thermal, and magnetic properties of metal/tcnq network polymers with extensive supramolecular interaction between layers. *Chem. Mater.* **1999**, 11,

736. (f) Segura, M.; Sanchez, L.; de Mendoza, J.; Martin, N.; Guldi, D. M. Hydrogen bonding interfaces in fullerene.TTF ensembles. *J. Am. Chem. Soc.* **2003**, 125, 15093−15100. (g) Gadde, S.; Shafiquil Islam, D.-M.; Wijesinghe, C. A.; Subbaiyan, N. K.; Zandler, M. E.; Araki, Y.; Ito, O.; D'Souza, F. Light-induced electron transfer of a supramolecular bis(zinc porphyrin)-fullerene triad constructed via a diacetylamidopyridine/uracil hydrogen-bonding motif. J. Phys. Chem. C 2007, 111, 12500−12503.

3. (a) Fourmigue´, M.; Uzelmeier, C. E.; Boubekeur, K.; Bartley, S. L.; Dunbar, K. R. Bis- and tetrakis-(diphenylphosphino)tetrathiafulvalenes as precursors of redox-active organic-inorganic polymeric networks. *J. Organomet. Chem.* **1997**, 529, 343. (b) Chen, Z.; Lohr, A.; Saha-Möller, C. R.; Würthner, F. Self -assembled π-stacks of functional dyes in solution: Structural and thermodynamic Features. *Chem. Soc. Rev*. **2009**, 38, 564−584. (c) Ariga, K.; Kunitake, T. Supramolecular Chemistry - Fundamentals and Applications; Springer-Verlag: Berlin/Heidelberg, **2006**. (d) Steed, J. W.; Atwood, J. L. Supramolecular Chemistry; John Wiley & Sons, Ltd: Chichester, U.K., **2009**. (e) Lehn, J.-M. Supramolecular Chemistry; Wiley-VCH Verlag GmbH & Co. KGaA: Weinheim, Germany, **1995**. (f) Walatka, V. Jr.; Perlstein, J. H. Temperature Dependence of the Electrical Conductivity of Single Crystal Quinolinium $(TCNQ)_2$. *Mol. Cryst. Liq. Cryst.* **1971**, *15*, 269-272.
4. (a) Minot, M. J.; Perlstein, J. H. Mixed-Valence Square Planar Complexes: A New Class of Solids with High Electrical Conductivity in One Dimension. *Phys. Rev. Lett.*, **1971**, *26*, 371-373. (b) Hunter, C. A.; Sanders, J. K. M. The Nature of π- π interactions. *J. Am. Chem. Soc.* **1990**, 112, 5525−5534. (c) Hoeben, F. J. M.; Jonkheijm, P.; Meijer, E. W.; Schenning, A. P. H. J. About supramolecular assemblies of π-conjugated Systems. *Chem. Rev.* **2005**, 105, 1491−1546. (d) Das, A.; Ghosh, S. Supramolecular Assemblies by Charge Transfer

Interactions between Donor and Acceptor Chromophores. *Angew. Chem., Int. Ed.* **2014**, 53, 2038−2054. (e) Menon, R., Yoon, C. O., Moses, D. & Heeger, A. J. In Handbook of Conducting Polymers. 2nd ed. Marcel Dekker, New York, **1998**.

5. (a) Heeger, A. J. The critical regime of the metal-insulator transition in conducting polymers: experimental studies. *Phys. Scr.*, **2002**, T102, 30–35. (b) Rathore, R.; Lindeman, S. V.; Kochi, J. K. Charge-transfer probes for molecular recognition via steric hindrance in donor-acceptor pairs. *J. Am. Chem. Soc.* **1997**, 119, 9393-9404. (c) Cowan, D. O.; Kaufman, F. *J. Am. Chem. Soc*. The Organic Solid State. Electron transfer in a mixed valence salt of biferrocene.**1970**, *92*, 219-220. (d) Cowan, D.O.; Pasternak, G.; Kaufman, F. Biological Electron Transport Systems. *Proc. Nat. Acad. Sci. U. S.* **1970**, *66*, 837-843.

6. (a) Bryce, M.R. Current Trends in Tetrathiafulvalene Chemistry: towards Increased Dimensionality. *J. Mater. Chem.* **1995**, *5*, 1481-1496. (b) Martin, N.; Segura, J.L.; Seoane, C. Design and Synthesis of TCNQ and DCNQ1 Type Electron Acceptor Molecules as Precursors for "Organic Metals". *J. Mater. Chem.* **1997**, *7*, 1661-1676. (c) Roncali, J. Linearly Extended π-donors: When Tetrathiafulvalene Meets Conjugated Oligomers and Polymers. *J. Mater. Chem.* **1997**, *7*, 2307-2321. (d) Robertson, N.; Cronin, L. Metal bis-1,2-dithiolene complexes in conducting or magnetic crystalline assemblies. *Coord. Chem. Rev.* **2002**, 227, 93-127. (e) Braga, D.; Grepioni, F.; Desiraju, G. R. Crystal engineering and organometallic architecture. *Chem. Rev.* **1998**, 98, 1375-1405.

7. (a) Geary, E. A. M.; Yellowlees, L. J.; Jack, L. A.; Oswald, I. D. H.; Parsons, S.; Hirata, N.; Durrant, J. R.; Robertson, N. Synthesis, structure, and properties of [Pt(II)(diimine)(dithiolate)] dyes with 3,3'-, 4,4'-, and 5,5'-disubstituted bipyridyl: applications in dye-sensitized solar cells. *Inorg. Chem.* **2005**, 44, 242. (b) O'Regan, B.;

Grätzel, M. A low-cost, high-efficiency solar cell based on dye-sensitized colloidal TiO_2 films. *Nature* **1991**, 353, 737. (c) Islam, A.; Sugihara, H.; Hara, K.; Singh, L. P.; Katoh, R.; Yanagida, M.; Takahashi, Y.; Murata, S.; Arakawa, H. Dye sensitization of nanocrystalline titanium dioxide with square planar platinum(II) diimine dithiolate complexes. *Inorg. Chem.* **2001**, 40, 5371. (d) Yella, A.; Lee, H.-W.; Tsao, H. N.; Yi, C.; Chandiran, A. K.; Nazeeruddin, M. K.; Diau, E. W-G.; Yeh, C.-Y.; Zakeeruddin, S. M.; Gratzel, M. Phorphyrin-sensitized solar cells with cobalt (II/III)-based redox electrolyte exceed 12 percent efficiency. *Science* **2011**, 334, 629. (e) Nazeeruddin, M. K.; De Angelis, F.; Fantacci, S.; Selloni, A.; Viscardi, G.; Liska, P.; Ito, S.; Takeru, B.; Gratzel, M. Combined experimental and DFT-TDDFT computational study of photoelectrochemical cell ruthenium sensitizers. *J. Am. Chem. Soc.* **2005**, 127, 16835. (f) Ghiassi, K. B.; Olmstead, M. M.; Balch, A. L. Orientational variation, solvate composition and molecular flexibility in well-ordered cocrystals of the fullerene C_{70} with bis(ethylenedithio)-tetrathiafulvalene. *Chem. Commun.*, **2013**, 49, 10721-10723. (g) Ghiassi, K. B.; Powers, X. B.; Chen, S. Y.; Aristov, M. M.; Balch, A. L.; Olmstead, M. M. Reluctant cocrystal growth of fullerenes with nickel dithiolene complexes. *Inorganica Chimica Acta.* 2018, 473, 1-8.

8. Tanaka, H.; Okano, Y.; Kobayashi, H.; Suzuki, W.; Kobayashi, A. A Three-dimensional Synthetic Metallic Crystal of Single-component Molecules. *Science* **2001**, *291*, 285-287.

9. (a) Smucker, B.W.; Hudson, J.M.; Omary, M.A.; Dunbar, K.R. Structural, Magnetic, and Optoelectronic Properties of (Diimine)(dithiolato)platinum(II) and –palladium(II) Complexes and Their Charge-transfer Adducts with Nitrile Acceptors. *Inorg. Chem.* **2003**, *42*, 4714-4723. (b) Browning, C.; Hudson, J. M.; Reinheimer, E. W.; Kuo, F.-L.; McDougald, R. N., Jr; Rabaâ, H.; Pan, H.; Bacsa, J.; Wang, X.; Dunbar, K. R.; Shepherd, N. D.; Omary, M. A. Synthesis, Spectroscopic Properties, and Photoconductivity of Black Absorbers Consisting of Pt

(Bipyridine)(Dithiolate) Charge Transfer Complexes in the Presence and Absence of Nitrofluorenone Acceptors. *J. Am. Chem. Soc.* 2014, *136*, 16185-16200. (c) For detailed theoretical insights about ref 9b, see: Cundari, T. R.; Chilukuri, B.; Hudson, J. M.; Minot, C.; Omary, M. A.; Rabaâ, H. Periodic and Molecular Modeling Study of Donor-Acceptor Interactions in (dbbpy)Pt(tdt)•(TENF) and [Pt(dbbpy)(tdt)]2•(TENF). *Organometallics* **2010**, *29*, 795-800.

10. (a) Chen, W. –H.; Reinheimer, E.W.; Dunbar, K.R.; Omary, M. A. Coarse and Fine Tuning of the Electronic Energies of Triimineplatinum(II) Square-planar Complexes. *Inorg. Chem.* **2006**, *45*, 2770-2772. (b) For detailed theoretical insights about ref 10a, see: Rabaâ, H.; Cundari, T. R.; Omary, M. A. Combined Tight Binding/DFT Investigation of the Electronic Structure of Triimine-Platinum(II)/TCNQ Extended Stacks: Theoretical Prediction of Metallic Behavior. Can. J. Chem. 2009, *87*, 775-783.

11. Coomber, A.T.; Beljonne, D.; Friend, R.H.; Brédas, J.K.; Charlton, A.; Robertson, N.; Underhill, A. E.; Kurmoo, M.; Day, P. Intermolecular Interactions in the Molecular Ferromagnetic $NH_4Ni(mnt)_2.H_2O$. *Nature* **1996**, *380*, 144-146.

12. (a) Olmstead, M. M.; Jiang, F.; Attar, S.; Balch, A. L. Alteration of the Aurophilic Interactions in Trimeric Gold (I) Compounds through Charge Transfer. Behavior of Solvoluminescent $Au_3(MeN{=}COMe)_3$ in the Presence of Electron Acceptors. *J. Am. Chem. Soc.* **2001**, *123*, 3260-3267. (b) Rawashdeh-Omary, M. A.; Omary, M. A.; Fackler, J. P., Jr.; Galassi, R.; Pietroni, B. R.; Burini, A. Chemistry and Optoelectronic Properties of Stacked Supramolecular Entities of Trinuclear Gold(I) Complexes Sandwiching Small Organic Acids. *J. Am. Chem. Soc.* **2001**, *123,* 9689-9691. (c) Burini, A.; Fackler, J. P., Jr.; Galassi, R.; Grant, T. A.; Omary, M. A.;

Rawashdeh-Omary, M. A.; Pietroni, B. R.; Staples, R. J. Supramolecular Chain Assemblies Formed by Interaction of a π- Molecular Acid Complex of Mercury with π-Base Trinuclear Gold Complexes. *J. Am. Chem. Soc.* **2000**, *122*, 11264-11265. (d) Burini, A.; Bravi, R.; Fackler, J. P., Jr.; Galassi, R.; Grant, T. A.; Omary. M. A.; Pietroni, B. R.; Staples, R. J. "Luminescent Chains Formed from Neutral, Triangular Gold Complexes Sandwiching Tl(I) and Ag(I). Structures of $\{Ag([Au(\mu\text{-}C2,N3\text{-}bzim)]_3)_2\}BF_4\odot CH_2Cl_2$, $\{Tl([Au(\mu\text{-}C2,N3\text{-}bzim)]_3)_2\}PF_6$ 0.5THF (bzim= 1-Benzylimidazolate), and $\{Tl([Au\ (\mu\text{-}C(OEt)NC_6H_4CH_3)]_3)_2\}PF_6$ THF, with MAu_6 ($M= Ag^+, Tl^+$) Cluster Cores", *Inorg. Chem.* **2000**, *39*, 3158-3165.

13. Alvarez, S.; Vicente, R.; Hoffman, R. Dimerization and Stacking in Transition-metal Bisdithiolenes and Tetrathiolates. *J. Am. Chem. Soc.* **1985**, *107*, 6253-6277.

14. (a) Omary, M. A.; Kassab, R. M.; Haneline, M. R.; Bjeirami, O. E.; Gabbaı¨, F. P. Enhancement of the phosphorescence of organic luminophores upon interaction with mercury trifuctional Lewis acid. *Inorg. Chem.* **2003**, 42, 2176. (b) Mohamed, A. A.; Rawashdeh-Omary, M. A.; Omary, M. A. Fackler, J. P. External heavy-atom effect of gold in a supramolecular acid-base π stack. *Dalton Trans.* **2005**, 15, 2597-2602. (c) Omary, M. A.; Mohamed, A. A.; Rawashdeh-omary, M. A.; Fackler, J. P. Photophysics of supramolecular binary stacks consisting of electron-rich trinuclear Au(I) complexes and organic electrophiles. *Coord. Chem. Rev.* **2005**, 249, 1372-1381. (d) Elbjeirami, O.; Rashdan, M. D.; Nesterov, V.; Rawashdeh-Omary, M. A. Structure and luminescence properties of a well-known macrometallocyclic trinuclear Au(I) complex and its adduct with a perfluorinated fluorophore showing cooperative anisotropic supramolecular interactions. *Dalton Trans.* **2010**, 39, 9465-9468. (e) Rawashdeh-Omary, M. A. Remarkable alteration of photophysical properties of

cyclic trinuclear complexes of monovalent coinage metals upon interactions with small organic molecules. *Comment Inorg. Chem.* **2013**, 33, 88-101.

15. Dias, H.; Rasika Dias, H.V.; Polach, S.A.; Wang, Z. Coinage Metal Comlexes of 3,5-bis(trifluoromethyl)pyrazolate Ligand Synthesis and Characterization of $\{[3,5\text{-}(CF_3)_2Pz]Cu\}_3$ and $\{[3,5\text{-}(CF_3)_2Pz]Ag\}_3$. *Journal of Fluorine Chemistry* **2000**, 163-169.

16. Bovio, B.; Bonati, F.; Banditelli, G. X-ray Crystal Structure of tris[μ-3,5-bis(trifluoromethyl)pyrazolato-N, N']trigold(I), a Compound Containing an Inorganic Nine-membered Ring. *Inorg. Chim. Acta*. **1984**, 25-33.

17. Galassi; R.; Ricci; S.; Burini; A.; Macchioni, A.; Rocchigiani, L.; Marmottini, F.; Tekarli, S.M.; Nesterov; V.N.; Omary, M.A. Solventless Supramolecular Chemistry via Vapor Diffusion of Volatile Small Molecules upon a New Trinuclear Silver(I)-Nitrated Pyrazolate Macrometalliccyclic Solid: An Experimental/ Theoritical Investigation of the Dipole/Quadrupole Chemisorption Phenomena. *Inorg. Chem*. **2013**, *52*, 14124-14137.

18. Bonati, F.; Burini, A.; Pietroni, B. R. Reactions of C-imidazolyllithium derivatives with Group Ib Compounds: tris[μ-(1-alkylimidazolato-N^3C^2)]trigold(I) and –silver(I). Crystal Structure of bis(1-benzylimidazolin-2-ylidene)gold(I)chloride. *J. Organomet. Chem.* **1989**, *375*, 147-160.

19. Bruker APEX2; Bruker AXS Inc.: Madison, WI, **2007**.

20. Bruker SAINT; Bruker AXS Inc.: Madison, WI, **2007**.

21. Bruker SADABS; Bruker AXS Inc.: Madison, WI, **2007**.

22. Sheldrick, G.M. SHELXTL, v. **2008/3**; Bruker Analytical X-ray: Madison, WI, **2008**.

23. (a) Hoffman, R.; Lipscomb, W. N. Theory of Polyhedral Molecules. I. Physical Factorizations of the Secular Equation. *J. Chem. Phys.* **1962**, *36*, 2179-2189. (b) Hoffman, R.; Lipscomb, W. N. Theory of Polyhedral Molecules. III. Population Analyses and Reactivities for the Carboranes. *J. Chem. Phys.* **1962**, *36*, 3489-3493. (c) Hoffman, R.; Lipscomb, W. N. Sequential Substitution Reactions on $B_{10}H_{10}$ and $B_{12}H_{12}$. *J. Chem. Phys.* **1963**, *37*, 520-523.

24. (a) Landrum, G. A.; Glassey, W. V. *YAeHMOP* (Yet another Extended Hückel Molecular Orbital Package); Cornell University: Ithaca, NY, **1995**, Version 3.0; freely available on the Web at http://sourceforge.net/projects/yaehmop/. (b) Hoffmann, R. Solids and Surfaces: A Chemist's View of Bonding in Extended Structures; VCH Publishers, Inc.: New York, **1988**.

25. (a) Ammeter, J. H.; Elian, M.; Summerville, R. H.; Hoffman, R. Counterintuitive Orbital Mixing in Semiempirical and Ab Initio Molecular Orbital Calculations. *J. Am. Chem. Soc.* **1978**, *100*, 3686-3692. (b) Whangbo, M.-H.; Hoffman, R. The band Structure of the Tetracyanoplatinate Chain. *J. Am. Chem. Soc.* **1978**, *100*, 6093.

26. (a) Lopes, E.B.; Alves, H.; Ribera, E.; Mas-Torrent, M.; Auban-Senzier, P.; Candell, E.; Henriques, R.T.; Almeida, M.; Molins, E.; Veciana, J.; Rovira, C.; Jerome, D. Electronic Localization in an Extreme 1-D Conductor: The Organic Salt $(TTDM\text{-}TTF)_2(Au(mnt)_2]$. *Eur. Phys. J. B* **2002**, *29*, 27-33. (b) M.J. Frisch, et al. Gaussian 09, Revision, A. I. Gaussian, Inc., Wallingford CT. **2009**.

27. Hay, P. J.; Wadt, W. R., Ab *initio* effective core potentials for molecular calculations. Potentials for the transition metal atoms Sc to Hg. *J. Chem. Phys.* **1985,** *82*, 270-283.

28. (a) Becke, A.D. A New Mixing of Hartree-Fock and Local-density Functional Theories. *J. Chem. Phys.* **1993**, *98*, 1372-1377. (b) Lee, C.; Yang, W.; Parr, R. G. Development of the Colle-Salvetti Correlation-energy Formula into a Functional of the Electron Density. *Phys. Rev.* **1998**, *B37*, 785-789.

29. Ahlrichs, R.; Häser, M.; Horn, H.; Kölmel, C. Electronic Structure Calculations on Workstation Computers: the Program System TURBOMOLE. *Chem. Phys. Lett.* **1989**, *162*,165–169.

30. Tekarli, S. M.; Cundari, T. R.; Omary, M. A. Rational Design of Macrometallocyclic Trinuclear Complexes with Superior π-Acidity and π -Basicity. *J. Am. Chem. Soc.* **2008**, 130, 1669-1675.

31. (a) Macchioni, A. Elucidation of the Solution Structures of Transition Metal Complex Ion Pairs by NOE NMR Experiments. *Eur.J.Inorg.Chem*. **2003**, 195-205. (b) Pregosin, P.S.; Kumar, P.G.A.; Fernandez, I. Pulsed Gradient Spin-echo (pgse) Diffusion and 1H, 19F Heteronuclear Overhauser Spectroscopy (HOESY) NMR Methods in Inorganic and Organometallic Chemistry: Something Old and Something New. *Chem. Rev.*, **2005**, *105*, 2977-2998. (c) Rocchigiani, L.; Macchioni, A. Disclosing the Multi-faceted World of Weakly InteInorg.racting Inorganic Systems by Means of NMR Spectroscopy. *Dalton Trans.*, **2016**, *45*, 2785.

32. (a) Bellachioma, G.; Binotti, B.; Cardaci, G.; Carfagna, C.; Macchioni, A.; Sabatini, S.; Zuccaccia, C. Solution Structure Investigations of Olefin Pd(II) and Pt(II) Complex Ion Pairs Bearing α-diimine Ligands by ^{19}F, ^{1}H-HOESY NMR. *Inorg. Chim. Acta* **2002**, *330*, 44-51. (b) Macchioni, A.; Magistrato, A.; Orabona, I.; Ruffo, F.; Rothlisberger, U.; Zuccaccia, C. Direct

Observation of an Equilibrium Between Two Anion-cation Orientations in Olefin Pt(II) Complex Ion HOESY NMR Spectroscopy. *New J. Chem*. **2003**, *27*, 455-458. (c) Ciancaleoni, G.; Biasiolo, L.; Bistoni, G.; Macchioni, A.; Tarantelli, F.; Zuccaccia, D.; Belpassi, L. NHC-Gold Alkyne Complexes: Influence of the Carbene Backbone on the Ion Pair Structure. *Organometallics*, **2013**, *32*, 4444-4447.

33. (a) Castiglione, F.; Appetecchi, G.B.; Passerini, S.; Panzeri, W.; Indelicato, S.; Mele, . Multiple Points of View of Heteronuclear NOE: Long Range vs Short Range Contacts in Pyrrolidinium Based Ionic Liquids in the Presence of Li Salts. *J. Mol. Liq*. **2015**, *210*, 215-222. (b) Khatun, S.; Castner, E.W. Photoinduced Bimolecular Electron transfer from Cyano Anions in Ionic Liquids. *J. Phys. Chem. B*, **2015**, *119*, 9225-9235.

34. Rocchigiani, L.; Ciancaleoni, G.; Zuccaccia, C.; Macchioni, A. Probing the Association of Frustrated Phosphine-Borane Lewis Pairs in Solution by NMR Spectroscopy. *J. Am. Chem. Soc.* **2014**, *136*, 112-115.

35. Zuccaccia, D.; Pirondini, L.; Pinalli, R.; Dalcanale, E.; Macchioni, A. Dynamic and Structural NMR Studies of Cavitand-Based Coordination. *J. Am. Chem. Soc.* **2005**, *127*, 7025-7032.

36. Burini, A.; Fackler, J.P.; Galassi, R.; Macchioni, A.; Omary, M.A.; Rawashdeh-Omary, M.A.; Pietroni, B.R.; Sabatini, S.; Zuccaccia, C. ^{19}F, ^{1}H-HOESY and PGSE NMR Studies of Neutral Trinuclear Complexes of Au^{I} and Hg^{II}: Evidence for Acid-Base Stacking in Solution. *J. Am. Chem. Soc.* **2002**, *124*, 4570-4571.

37. Weiss-Errico, M. J.; Ghiviriga, I.; O'Shea, K. E. ^{19}F NMR Characterization of Encapsulation of Emerging Perfluoroethercarboxylic Acids by Cyclodextrins. J. Phys. Chem. B, **2017**, *121*, 8359-8366.

38. Ciancaleoni, G.; Bertani, R.; Rocchigiani, L.; Sgarbossa, P.; Zuccaccia, C.; Macchioni, A. Discriminating Halogen-Bonding from Other Noncovalent Interactions by Combined NOE NMR/DFT Approach. *Chem. Eur. J.*, **2015**, *21*, 440-447.

39. (a) Stauffer, D. A.; Barrans, R. E. Jr.; Dougherty, D.A. Concerning the Thermodynamics of molecular Recognition in Aqueous and Organic Media. Evidence for Significant Heat Capacity Effects. *J. Org. Chem.* **1990**, *55*, 2762-2767. (b) Simova, S.; Berger, S. Diffusion Measurements vs. Chemical Shift Titration for Determination of Association Constants on the Example of Camphor-Cyclodextrin Complexes. J. *Incl. Phenom. Macrocycl. Chem.*, **2005**, *53*, 163-170.

40. (a) Rocchigiani, L.; Zuccaccia, C.; Zuccaccia, D.; Macchioni, A. Self-aggregation Tendency of Zirconocenium Ion Pairs Which Model Polymer-chain-carrying Species in Aromatic and Aliphatic Solvents with Low Polarity. *Chem. Eur. J.*, **2008**, *14*, 6589-6592. (b) Rocchigiani, L.; Bellachioma, G.; Ciancaleoni, G.; Macchioni, A.; Zuccaccia, D.; Zuccaccia, C. Syntheis, Characterization, Interionic Structure, and Self-Aggregation Tendency of Zirconnaziridinium Salts Bearing Long Alkyl Chains. *Organometallics*, **2011**, *30*, 100-114.

41. (a) Combettes, L. E.; Clausen-Thue, P.; King, M. A.; Odell, B.; Thompson, A. L.; Gouverneur, V.; Claridge, T. D. W. *Chem. Eur. J.* **2012**, *18*, 13133 – 13141. (b) Neuhaus, D.; Williamson, M. *The Nuclear Overhauser Effect in Structural and Conformational Analysis*; VCH Publishers: New York, 1989.

42. (a)Omary, M. A.; Rawashdeh-Omary, M. A.; Gonser, M. W. A.; Elbjeirami, O.; Grimes, T.; Cundari, T. R.; Diyabalanage, H, V. K.; Palehepitiya Gamage, C. S.; Dias, H. V. R. "Metal Effect on the Supramolecular Structure, Photophysics, and Acid/Base Character of Trinuclear Pyrazolato Coinage Metal Complexes", *Inorg. Chem.* **2005***, 44*, 8200-8210. (b) Ghimire, M.M.; Nesterov, V. N.; Omary, M. A. Remarkable Aurophilicity and Photoluminescence Thermochromism in a Homoleptic Cyclic Trinuclear Gold(I) Imidazolate Complex. *Inorg. Chem.*, **2017**, 56 (20), 12086–12089. (c) Galassi, R.; Ghimire, M. M.; Otten, B. M.; Ricci, S.; McDougald, R. N., Jr.; Almotawa, R. M.; Alhmoud, D.; Ivy, J. F.; Rawashdeh, A. M.; Nesterov, V. N.; Reinheimer, E. W.; Daniels, L. M.; Burini, A.; Omary, M. A. Cupriphication of Gold to Sensitize d^{10}-d^{10} Metal-Metal Bonds and Near Unity Phosphorescence Quantum Yields. *Proc. Natl. Acad. Sci.* U. S. A. **2017**, 114, E5042−E5051. (d) Chilukuri, B.; McDougald, R. N., Jr.; Ghimire, M. M.; Nesterov, V. N.; Mazur, U.; Omary, M. A.; Hipps, K. W. Polymorphic, Porous, and Host−Guest Nanostructures Directed by Monolayer−Substrate Interactions: Epitaxial Self-Assembly Study of Cyclic Trinuclear Au(I) Complexes on HOPG at the Solution−Solid Interface. *J. Phys. Chem. C,* **2015**, 119, 24844−24858.

TOC Graphical Abstract and synopsis

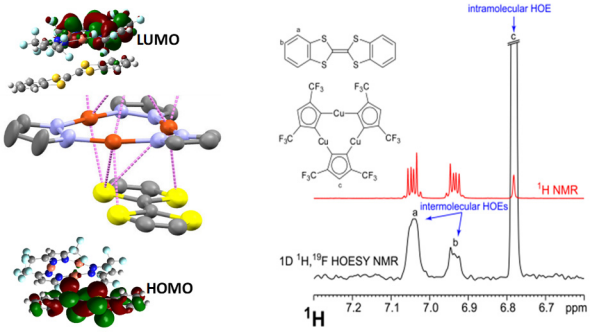

Binary donor-acceptor adducts obtained by the reaction of π-acidic trinuclear coinage metal cyclic compounds with electron-donating organic compounds (tetrathiafulvalene derivatives) have been found to exhibit remarkable supramolecular structures in both the solid state and solution. The detailed experimental and theoretical characterization of the adducts provide insights on the nature of the donor/acceptor supramolecular bonding interactions and give rise to remarkable magneto-opto-electronic properties, establishing the basis for future potential applications in molecular electronic devices.